ACS APPLIED NANO MATERIALS

www.acsanm.org Review

Review of Fiber-Based Three-Dimensional Printing for Applications Ranging from Nanoscale Nanoparticle Alignment to Macroscale Patterning

Weiheng Xu, Yuxiang Zhu, Dharneedar Ravichandran, Sayli Jambhulkar, Mounika Kakarla, Mohammed Bawareth, Shantanu Lanke, and Kenan Song*

Cite This: *ACS Appl. Nano Mater.* 2021, 4, 7538–7562 Read Online

ACCESS | Metrics & More | Article Recommendations

ABSTRACT: The field of additive manufacturing (AM) has witnessed spectacular growth in the past 4 decades because of its revolutionary processing mechanism in combining bottom-up and top-down approaches. Many have speculated that it will challenge traditional fabrication methods as the fourth industrial revolution. Among the subfields of three-dimensional (3D) printing, extrusion-based direct ink writing (DIW) is known for its vast material choices, high design flexibility, and acceptable cost efficiency to print many urgently demanded material systems, such as hydrogels or aerogels, nanoparticle suspensions, composite mixtures, liquid crystals, and liquid metals. Furthermore, the DIW's ability to construct complex architectures or hierarchies also contributes to broader applications across different fields, including intelligent robotics, energy generation and storage devices, biomedical implants, and sustainability systems. This review provides a comprehensive summary of recent advances in DIW development, focusing on engineered patterns at different scales, namely, nanoparticle alignment, one-dimensional (1D) fiber microstructure manipulation, and macroscale two-dimensional (2D)/3D spatial patterning. It highlights the hierarchies from nanoscale particle orientations to macroscale long-range-ordered structures. Finally, technical barriers and significant challenges prohibiting DIW for broader applications or impeding fundamental research to industrial commercialization are discussed.

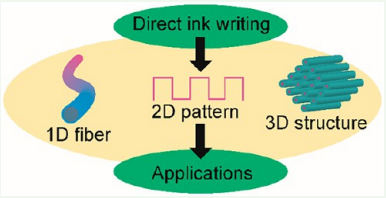

KEYWORDS: *fibers, direct ink writing, 3D printing, nanoparticles, alignment, nanocomposites*

1. INTRODUCTION

Textiles are everywhere in our modern society. Human history has seen decoration for aesthetic and comfort purposes at home or in public as the traditional role of textiles, worn as clothing for protection and self-expression or structural elements for shelters. Nevertheless, these perceptions toward textiles have evolved, with the fabric materials having an increasing trend of not only serving as a surface or being interpreted graphically but also functioning with specific purposes. The unique physical properties of textile materials (e.g., softness, stretchability, scalability) make them perfect media for broad applications, such as structural substrates, thermal management, wearable electronics, optical reflectors, biosensors, and energy storage devices.[1−5] Fiber is the most fundamental building block for all textile materials. The one-dimensional (1D) fiber structure offers many fascinating features, including high flexibility, excellent mechanical properties, large surface-area-to-volume ratios, and high inherent anisotropic characteristics. Its standard fabrication techniques include dry spinning, wet spinning, gel spinning, melt spinning, and electrospinning.[6−9] Through weaving, knitting, braiding, and nonwoven methods, 1D fibers are eventually transformed into two-dimensional (2D) film/membrane or three-dimensional (3D) mesh/mat structures. To further equip these fabrics with functionalities, general methods including coating (e.g., spraying, dipping, casting, and doctor blading) and plating (e.g., electroless depositing, thermal depositing, and magnetron sputtering) of nanomaterials have been widely used.[10−13] Nevertheless, these additional postspinning fabrication steps can significantly limit production efficiency, pose challenges to material selections, and cause difficulties for desirable geometry.

Currently, with the broader accessibility of additive manufacturing (AM), also known as 3D printing, bottom-up manufacturing has been recognized as the fourth industrial revolution for its numerous advantages over conventional manufacturing (known as subtractive manufacturing).[14] 3D printing methods can be primarily divided into seven categories according to ASTM definition, namely, (1) material

Received: May 28, 2021
Accepted: August 5, 2021
Published: August 17, 2021

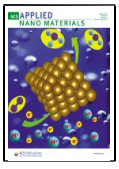

https://doi.org/10.1021/acsanm.1c01408
ACS Appl. Nano Mater. 2021, 4, 7538–7562

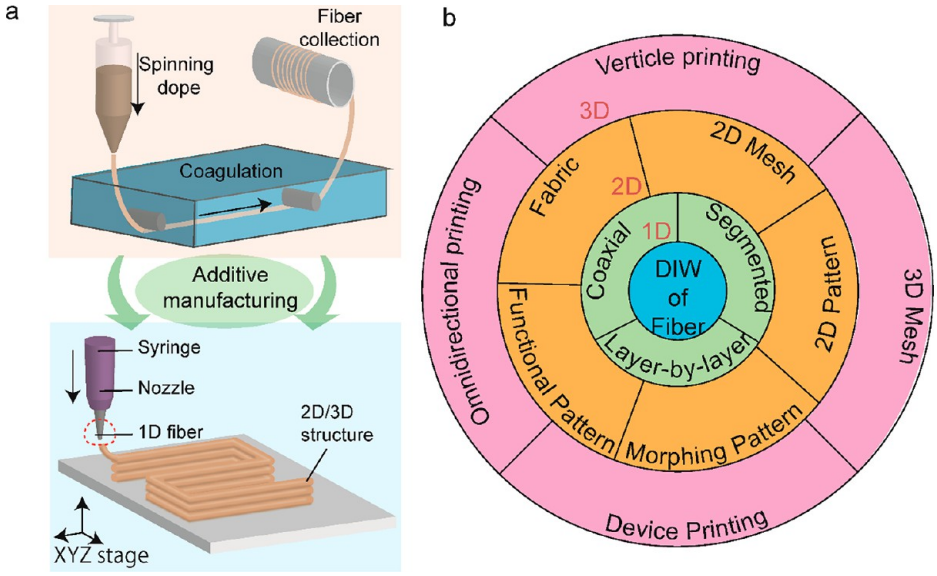

Figure 1. (a) Working mechanism between extrusion-based fiber spinning and DIW. (b) Structure of this review paper, including DIW of fiber-based materials of 1D, 2D, and 3D structures.

extrusion, (2) material jetting, (3) binder jetting, (4) sheet lamination, (5) vat photopolymerization, (6) powder bed fusion (PBF), and (7) directed energy deposition.[15] Each type has its advantages and specialties, which have been summarized in previous reviews.[16] For instance, photocuring-based methods include stereolithography (SLA), digital light processing (DLP), and especially two-photon/multiphoton polymerization (2/MPP), offering higher spatial resolution (e.g., ∼100 nm for 2/MPP) and better isotropic properties than other 3D printing approaches.[17] Inkjet-based methods of MultiJet/PolyJet printing or electrohydrodynamic (EHD) printing allow pure nanoparticle deposition and multimaterial compatibility.[18] PBF-based methods of selective laser sintering (SLS) and selective laser melting (SLM) often utilize high-intensity power lasers primarily suitable for metal processing (e.g., steels, titanium, nickel-based, cobalt chrome, and aluminum alloys).[19] However, these methods rely on raw materials of monomers, suspensions, and powders that created many complexities in the fabrication of continuous material forms free of voids along individual printing lines or within individual additive layers. On the contrary, extrusion-based methods, including direct ink writing (DIW) and fused deposition modeling (FDM), share the same fundamental principle as fiber-spinning techniques and rely on a cost-efficient extrusion strategy, making them the optimum 3D printing option for 1D fiber and fiber-relevant (i.e., filaments, textiles, and fabrics) materials. In FDM, a thermoplastic polymer filament is frequently extruded through a heated nozzle and melted into a semimolten form to construct the desired structures in a layer-by-layer fashion. The quality of the printed parts mainly depends on the filament properties (e.g., material types and polymer transition temperatures) and printing parameters (e.g., temperature and speed). Filament materials can be divided into commodity grade, engineering grade, and high-performance grade, depending on their thermal, mechanical, and chemical stability.[20] Filament compositing, such as the incorporation of reinforcement particles, short fillers, or continuous fibers, is one way to enhance the filament properties. These fillers' uniform dispersion and volume concentration play significant roles in the degree of mechanical enhancement because they may lead to defects and nonuniform filament deposition without careful preprocessing or postprocessing.[21] Printing parameters such as the printing speed and print nozzle/bed/chamber temperatures also lead to different interlayer adhesion, void size, porosity, and residue stress.[22] Many reviews, including recent ones by Wickramasinghe et al.,[23] Penumakala et al.,[24] Mollica et al.,[21] and Gou et al.,[25] have explicitly introduced the FDM method and its applications; therefore, FDM methods will be excluded from this review.

DIW is compatible with a wide variety of materials, providing a manufacturing platform for multimaterial-incorporated composites or hybrids that other 3D printing methods find impossible or challenging to process. Because of the growing trend of DIW fiber-based materials, this review paper covers transferable technologies between existing fiber-spinning techniques and DIW-based AM (Figure 1a). Our summary focuses on extrusion-based DIW printing with the unique ability to produce fibrous structures for functional system and device applications. We start with a brief introduction of DIW procedures and manufacturing features, followed by material manufacturing at different scales (Figure 1b), namely, (i) nanoscale processing with shear-stress-induced nanoparticle alignment (feature size <500 nm), (ii) microscale fabrication for intricate fiber structures (feature size between 500 nm to 1 mm), and (iii) large-area or large-volume macroscale manufacturing for 2D/3D spatial patterning (feature size >1 mm), before concluding with future perspectives.

2. INTRODUCTION TO DIW 3D PRINTING

DIW was first reported by Cesarano and Calvert when they filed a patent at Sandia National Laboratories on October 28, 1997[26] and has been developed tremendously over the past 20 years. In the DIW process, materials are extruded in a simple form of ink through nozzles with a controllable rate. Through programming of defined paths and utilization of a computer-controlled translation stage, 3D structures are constructible in a dot-by-dot, line-by-line, or layer-by-layer fashion (Figure 1a). The resolution of printed parts is controlled by choosing

https://doi.org/10.1021/acsanm.1c01408
ACS Appl. Nano Mater. 2021, 4, 7538−7562

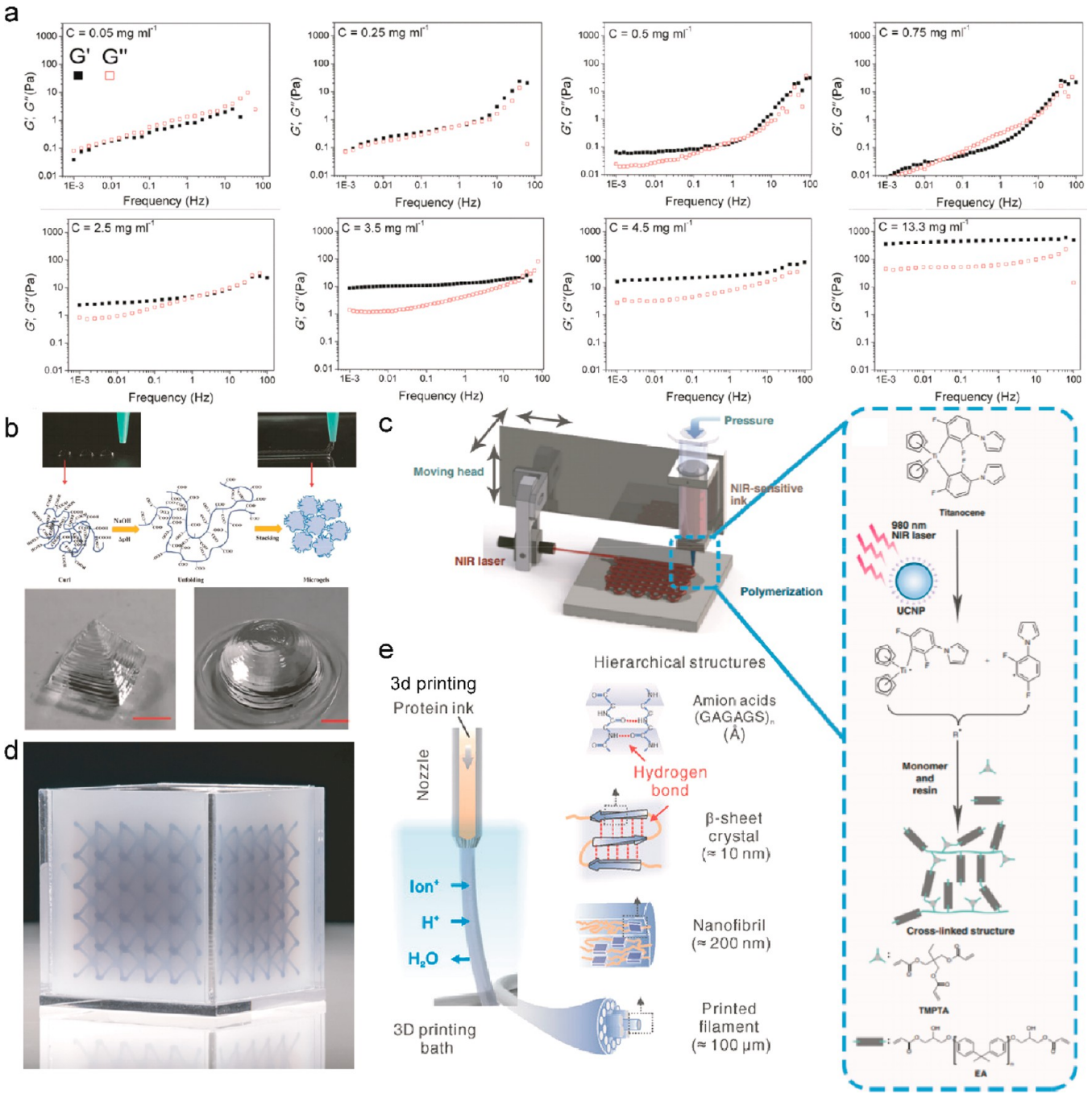

Figure 2. (a) Storage and loss moduli (filled and open squares, respectively) of GO suspensions as a function of the varying frequencies guiding ink preparations during DIW printing. Reproduced with permission from ref28. Copyright 2014 Royal Society of Chemistry. (b) Schematic of the fluid-to-gel transition of Carbomer-enabled ink by changing pH (ΔpH). Reproduced with permission from ref 29. Copyright 2019 Wiley-VCH. (c) Scheme of a NIR-induced DIW setup with a zoomed-in section showing structures and monomer-to-polymer reactions applied in NIR-induced DIW printing. Reproduced with permission from ref 30. Copyright 2020 Springer Nature. (d) Optical image of EMB3D-printed architectures. Reproduced with permission from ref 31. Copyright 2018 American Chemical Society. (e) EMB3D printing uses a rationally devised aqueous salt bath to direct molecular assembly for the construction of 3D-ordered and hierarchical structures, with a coagulation bath converting liquid inks to solid fibers and bridging the atomic-scale bonding to nanoscale molecular morphologies to macroscale filaments. Reproduced with permission from ref 32. Copyright 2020 Wiley-VCH.

different nozzle sizes and defining the printing parameters (e.g., varying the deposition environment and tuning the printing ink rheology). DIW printing has broader material selections than other 3D printing techniques (i.e., polyelectrolytes, colloids, solutions, gels, and composites for DIW versus limited monomers for SLA, small particle dispersions for inkjet, or fine powders for PBF). Multimaterial printing inks often compose solvents, binders, additives, and fillers, diversifying in metals, ceramics, polymers, and their composites. Because of its simple extrusion or dripping mechanism, DIW is a user-friendly and cost-efficient technique for the fabrication of functional nanocomposites at either bench- or industrial-scale manufacturing.

https://doi.org/10.1021/acsanm.1c01408
ACS Appl. Nano Mater. 2021, 4, 7538−7562

The rheological behavior of printing inks for the DIW process is one of the most crucial parameters in the successful construction of the desired geometry and performance. These inks need to possess acceptable shear-thinning and yield stress properties, typically with sufficient yield stress (τ > 200 Pa) and a high-enough storage modulus (G' > 1000 Pa).[27] During the extrusion process, ink should easily flow under shear stress to avoid any jamming in the nozzle. Upon exiting the nozzle, the printed ink should possess high elastic properties to maintain the structure without collapsing. Nevertheless, tuning such viscoelastic properties can be challenging because the magnitude of τ cannot exceed a specific limit that would form crevices beneath/behind the translating nozzle, leading to defects (e.g., voids and debonding). An extremely high modulus also has a tendency toward clogging and jamming depending on the nozzle and nanoparticle sizes.

Some nanoparticle additives are effective rheology reducers, and an understanding of their influences on the ink-flow behavior is required for successful 3D printing. The oscillatory rheology test is a commonly used quantitative method to determine these composite fluid properties. By analysis of the tan δ value, a ratio between the storage modulus (G') and loss modulus (G''), as a function of the oscillation frequency (Figure 2a), the printability of the ink is predictable. The higher-frequency range corresponds to the condition during extrusion, and the lower-frequency range corresponds to the early stage when ink first exits the printing nozzle. Optimizing the nanoparticle concentrations is a commonly used method to achieve DIW printability.[28,33−35] As shown in Figure 2a, the rheological requirement was satisfied by increasing the graphene oxide (GO) concentration from 0.05 to 13.3 mg mL^{-1}.[28] At lower concentrations up to 0.25 mg mL^{-1}, the relatively higher G'' value indicates a more liquidlike behavior with low yield stress. With an increase of the GO concentration up to 4.5 mg mL^{-1}, the dominating G' value at low frequency indicates a solidlike behavior, yet the storage modulus (≈10 Pa) is low for self-supporting structures. At 13.3 mg mL^{-1}, the higher storage modulus and more solidlike behavior ensure free-standing structures upon printing, while the higher G'' at higher frequency promotes better flowability during extrusion.[28] Clay minerals, such as halloysite nanotubes, palygorskite, or kaolinite, have also been widely used as rheology modifiers. Their biocompatibility makes them ideal candidates for DIW of biomaterials, a dominant application of DIW in biomedical and pharmaceutical areas.[36−39]

Other rheology modifiers effective for reduced fluid viscosity include molecular and ionic binders including polymers [e.g., hydroxypropyl methylcellulose (HPCM),[40] Carbomer[29]], hydrophilic nonionic surfactant copolymers (e.g., Pluronic F127),[41,42] and soluble inorganic precursor ions [e.g., chalcogenidometallate (ChaM)].[43] In the work by Yang and others, Carbomer, a cross-linked high-molecular-weight polymer of acrylic acid, transforms its molecular chains from curly to clustered structure after dispersion in water, showing a fluid-to-gel transition for DIW (Figure 2b).[29] For relatively low yield-stress materials with small-concentration nanoparticle filling, applying a curing agent is an alternative strategy.[34,44−47] Lewis and others developed an all-3D-printed lithium-ion battery containing cathode, anode, packaging, and separator.[48] The storage modulus of the separator ink was around 1 kPa, i.e., 10 and 1000 orders of magnitude smaller than those of the packaging and electrode material inks, respectively. To print batteries with such properties, they mixed ethoxylated trimethylolpropane triacrylate (ETPTA), Al_2O_3 particles, and lithium salt before cross-linking the mixture to achieve the required yield stress with the assistance of UV curing.[48] However, UV-based 3D printing has a trade-off between the required curing intensity and the effectiveness range. Recently, Liu et al. developed a near-infrared (NIR) laser-assisted DIW process to overcome this barrier. By applying a 980 nm NIR laser, they successfully solidified deposited filaments up to 4 mm (Figure 2c).[30] Other ink property-related methods include thermal cross-linking,[49] optimization of the uniformity and geometry of the nanoparticles,[50] and volatile solvent-based thixotropic materials.[51]

Nevertheless, tuning the viscoelastic properties of DIW inks can be challenging, especially for compliant, soft, or biological materials. Research regarding DIW-depositing materials in a medium that supports the printed part's structure has rapidly increased in recent years. Such a strategy is often associated with printing such soft inks as silicone, hydrogel, colloids, and living cells.[52−54] Because the viscoelastic properties for such materials have limited tunability, the support medium's viscoelastic properties became the study focus. The supporting material can be printed nanocrystals,[55] granule gels,[56] or a yield-stress liquid.[57] Lewis's group developed the embedded three-dimensional (EMB3D) printing technique, which utilized poly(dimethylsiloxane) (PDMS) and SE 1700 (composition of ∼20 wt % fumed silica) as the viscoplastic matrix for hosting Pluronic F127 in water for cell culture applications.[31] DIW in a coagulation bath is also a feasible solution for inks with low yield stress (Figure 2d). As the inks extrude into a reservoir containing nonsolvent liquids, the ink solvent and coagulation nonsolvent go through an exchanging process to form a more solid gel or solid structure. For example, cellulose is a sustainable natural resource for a wide range of applications. However, the concentration of cellulose nanocrystals (CNCs) added to DIW inks is limited, e.g., typically under 6.6 vol % for unmodified CNCs in a polymer matrix and 1.3−2.6 vol % for cellulose nanofibers dispersed in water, which easily collapses and spreads on printing substrates.[58,59] Using the coagulation process, highly flexible 3D-printed CNC structures are printable with low-modulus inks (G = 20 Pa).[60] The coagulation process has also shown benefits in the assembly of protein molecules. Kaplan's group showed that, by applying artificial aqueous solutions containing inorganic salts [i.e., 0.5 M dipotassium phosphate (K_2HPO_{4x}) and 4 M sodium chloride (NaCl)], silk-spinning conditions were recreated from spiders and silkworms (Figure 2e).[32] Upon further combination with 3D printing, a hierarchical assembly of silk fibroin (SF) into 3D macroscale architectures with intrinsic biocompatibility, mechanical strength, and the desired shape complexity was achieved.[32]

3. NANOSCALE NANOPARTICLE ALIGNMENT

Fibrous structure materials are known for their anisotropic properties for mechanical, electrical, and thermal applications.[61−65] For polymer nanoparticle composites, controlling the filler particles' spatial orientation is crucial for many applications. For instance, the mechanical reinforcement efficiency (eqs 1−6) for nanoparticle-filled polymer fibers is highly dependent on the Krenchel orientation factor (η_o; eq 3), which is calculated through the average angles between each nanoparticle axis and the fiber axis.[66,67]

$$E_c = E_m V_m + \eta_o \eta_f E_f V_f \quad (1)$$

https://doi.org/10.1021/acsanm.1c01408
ACS Appl. Nano Mater. 2021, 4, 7538−7562

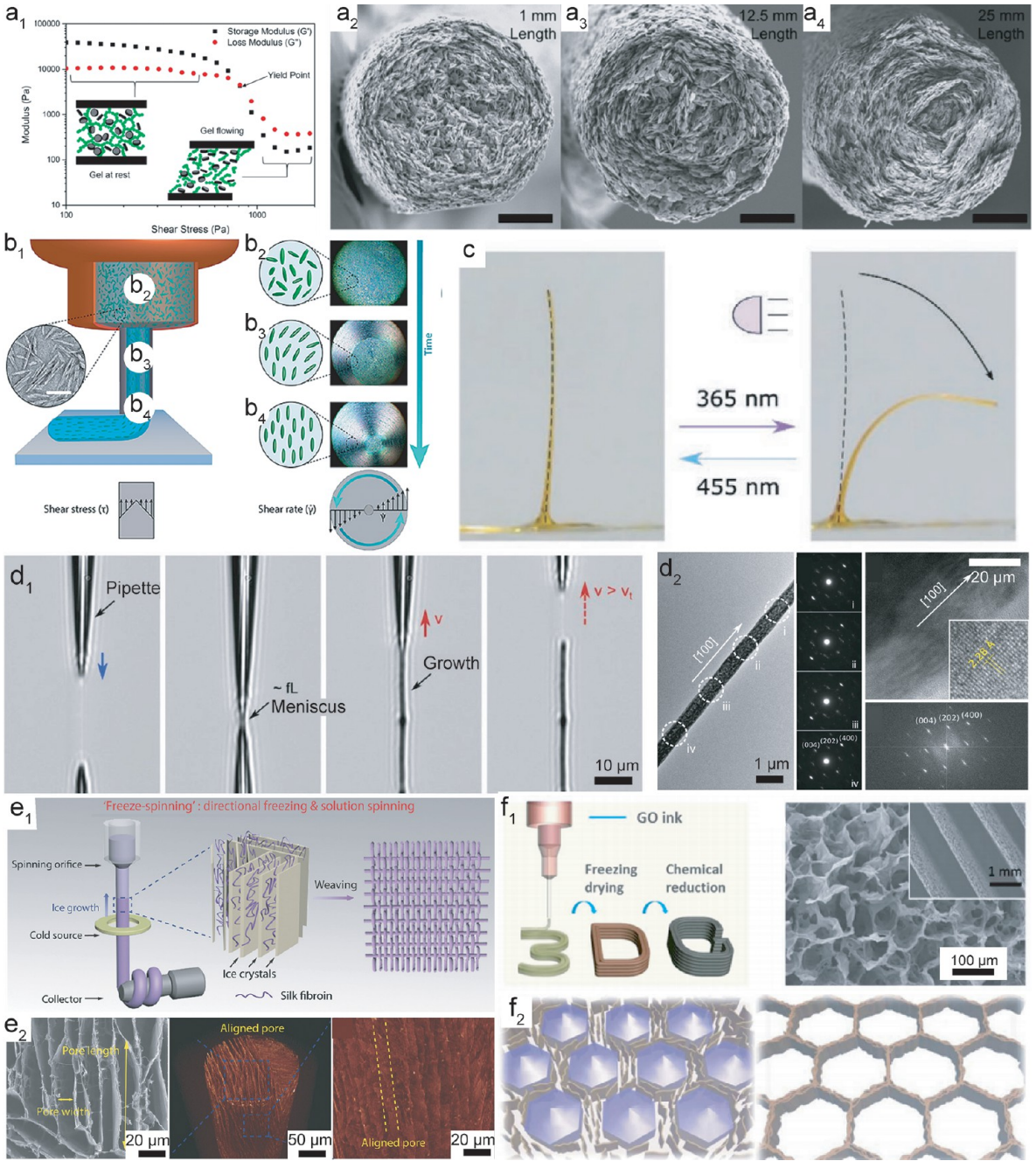

Figure 3. Nanoparticle alignment in a DIW-printed fibrous structure. (a_1) Dynamic mechanical analysis of the platelet-laden printing paste showing the paste stiffness and yield stress. (a_{2-4}) SEM images of filaments printed using different nozzle sizes, showing the nozzle length effect on the level of concentric platelet alignment. Scale bar: 30 μm. Reproduced with permission from ref 71. Copyright 2017 Springer Nature. (b_1) CNCs aligned during shearing in a DIW process. (b_2) Randomly organized CNC in the cartridge, (b_3) shear-induced alignment during extrusion through the nozzle, and (b_4) the final oriented extruded segment. Reproduced with permission from ref 72. Copyright 2018 American Chemical Society. (c) Side views of bending and unbending behaviors of LCs after irradiation with 365 and 455 nm light. Reproduced with permission from ref 75. Copyright 2020 Wiley-VCH. (d_1) Printing mechanism of the meniscus-guided method with (d_2) showing TEM images confirming the growth of perovskite in the [100] direction. Reproduced with permission from ref 94. Copyright 2019 Wiley-VCH. (e_1) Printing mechanism of freeze-drying with fiber spinning with (e_2) continuously aligned pores. Reproduced with permission from ref 106. Copyright 2018 Wiley-VCH. (f_1) Freeze-drying and DIW of GO supercapacitors with (f_2) the working principle of aligned GO. Reproduced with permission from ref 107. Copyright 2017 Royal Society of Chemistry.

$$\sigma_c = \sigma_m V_m + \eta_o \eta_f \sigma_f V_f \quad (2)$$

$$\eta_o = \frac{\int_0^{1/2\pi} I(\phi) \cos^4 \phi \, d\phi}{\int_0^{1/2\pi} I(\phi) \, d\phi} \quad (3)$$

$$\eta_f = 1 - \frac{\tanh(na)}{na} \quad (4)$$

$$n = \sqrt{\frac{2G_m}{E_f \ln\left(\frac{2R}{d}\right)}} \quad (5)$$

https://doi.org/10.1021/acsanm.1c01408
ACS Appl. Nano Mater. 2021, 4, 7538−7562

$$a = l/d \quad (6)$$

Here E_c, E_m, and E_f are the moduli values for the composites, polymer matrix, and reinforcement fillers, respectively. σ_c, σ_m, and σ_f are the strength values for the composites, polymer matrix, and reinforcement fillers, respectively. V_m and V_f are the volume fractions for the polymer matrix and reinforcement particles, respectively. The length factor (η_f) is related to the mechanics of the composite phases and distribution of the particles. R and d are the quasi-radius and distance between the nanoparticles. The orientation factor (η_o) is calculatable via the $I(\Phi)$ measurable via X-ray diffraction or neutron scattering by a Gaussian or Lorentzian distribution as a function of Φ.

Traditional methods such as dry spinning, wet spinning, dry-jet-wet spinning, orifice spinning, and microfluid spinning can facilitate nanoparticle alignment with the shear stress generated during fiber formation dynamics.[5,68−70] DIW of a fibrous structure also benefits from a similar mechanism; because a wide variety of materials are extruded from the print nozzle, their preferential alignment would benefit their structural and functional properties. Nanoparticle alignment is usually accompanied by shear-thinning behavior, as described and experimentally observed in Figure 3a$_1$. In this study conducted by Feilden's group, before printing, alumina platelet nanoparticles tend to be dispersed in the polymer matrix with no preferential orientation; this is indicated in the linear plateau region below the yield point at 885 Pa and stiffness at 38 kPa.[71] Because of the percolating networks of the anisotropic particles, the finite yield stress prohibited the ink's flowability. With an increase in the shear stress above the yield stress, the shear-thinning behavior begins and accompanies a decrease in the ink's modulus. The randomly dispersed nanoparticles begin to align themselves in the flow direction of the polymer binder. The cross-sectional scanning electron microscopy (SEM) images of the printed fiber filaments of different extrusion lengths shown in Figure 3a$_{2-4}$ indicate the platelet alignment. Each sample consists of a more oriented sheath layer and a more randomly oriented core layer. The area of the core layer gradually shrinks with an increase in the extrusion length. This longer extrusion path−more aligned platelets phenomenon is consistent with Studart's investigation into CNC composites.[72] Via in situ polarization rheology observations, Studart developed a systematic understanding of the CNC alignment at different phases of DIW printing; namely, the CNC particle alignment scales inversely with the applied shear rate and directly with the particle concentrations (Figure 3b$_{1-4}$).[72]

Through the alignment of different materials, DIW can enrich different functionalities (e.g., intelligent behaviors, mechanical reinforcement, and thermal management) to 3D-printed objects. For example, the liquid-crystal (LC) material known for its long-range orientational or positional organization at the molecular level as a function of the environmental conditions has broad applications in stimuli-responsive systems (e.g., soft robotics).[73,74] Major advantages of LC-based actuators include their high degree of actuation freedom responding to the external environment (e.g., aqueous or nonaqueous conditions and mechanical or stress-free programming). However, they need to be cross-linked in an aligned state. Schenning's group showed that, through shear thinning, DIW of a LC polymer resulted in molecular alignment with confirmation from 2D small-angle X-ray scattering (Figure 3c$_{1-3}$). A light-induced smectic C-to-smectic A phase transition directly results from the macroscopically aligned mesogen, which provided anisotropic expansion. The printed fiber demonstrated actuation behavior via temperature and light stimulus.[75]

CNCs with a high aspect ratio (length-to-diameter ratio of 10−70) gained much attention as mechanical reinforcement fillers for 3D printing.[76−79] Their high anisotropic properties usually originate from a high degree of alignment. Lewis's group has shown that the critical radius (r_c) for CNC nanoparticles to undergo shear-assisted orientation is dependent on three parameters: extrusion pressure (ΔP), nozzle length (L), and CNC concentrations.[34] An increase in ΔP would result in a lower r_c at the same CNC concentration, and an increase in the CNC concentration would lead to a higher r_c at constant ΔP. Printing of a 20 wt % CNC/water suspension successfully generates different architectures composed of filamentary features.[34] As water evaporates, the remaining CNC particles maintain their crystalline order, as proven by optical microscopy in a cross-polarized light mode. The 3D-printed structure shows a much smaller length scale of the birefringence effect than solution-cast films, reflecting the preferential orientation of CNCs via 3D printing versus the casted samples without CNC alignment.[34]

The simple mechanism for nanoparticle alignment in DIW also attracted much attention for 2D nanoparticles, such as MXene platelets, boron nitride (BN) nanosheets, and graphene layers.[80−83] Shahbazian-Yassar et al. developed a DIW-based, poly(ethylene oxide) (PEO) silane-treated hexagonal boron nitride (s-hBN) composite polymer electrolyte.[84] Through shear-induced alignment, s-hBN showed higher alignment in the printed direction, as shown by the IR images.[84] The alignment of the thermally conductive s-hBN avoided localized temperature accumulation, which resulted in lower lithium dendrite growth and potentially reduced internal shorting.[85]

Meniscus-guided alignment has often been used in dip coating, blade coating, and slot die coating, where nanoparticles or polymer chains are guided by viscous force during deposition.[86−90] Such a technique has also been combined with DIW in depositing metallic nanowires,[91] polymers,[92,93] perovskites,[94,95] and carbon-based materials.[96−98] For example, Kim et al. demonstrated the alignment of crystalline perovskite nanowires by DIW of methylammonium iodide and lead(II) iodide dissolved in *N*,*N*-dimethylformamide (DMF).[94] Figure 3d$_1$ illustrates this printing process as the ink was first extruded through a micropipette with a diameter of 600 nm onto a silicon substrate. When the micropipette was physically contacted with the substrate, the wetted surface formed the meniscus. As the micropipette was moved upward, DMF started to evaporate, leading to crystallization of the perovskite. Transmission electron microscopy (TEM) confirmed the preferred growth of the nanowires in the [100] direction, followed by the printing direction (Figure 3d$_2$).[94] Such a combination of meniscus-guided printing and DIW promotes the aligned growth of perovskite crystals at the nanoscale and breaks the limit of in-plane fabrication techniques.

Freeze-drying, also referred to as ice-templating or freeze-casting, has often been used to construct a 3D network structure for thermal insulation, battery electrode, and other functional applications.[99−105] By the utilization of lamellar ice crystals as a template, different polymers or ceramics are assembled in a unidirectional pattern. This biomimetic approach learns from nature when seawater forms ice and repels nonfreezing substances (e.g., salts and organics), which

https://doi.org/10.1021/acsanm.1c01408
ACS Appl. Nano Mater. 2021, 4, 7538−7562

Table 1. Polymer/Nanoparticle Composites with Different Hierarchical Structures for Varying Applications[a]

fiber structure	2D/3D pattern	materials: polymers	materials: solvents	materials: particles	applications	ref
coaxial	2D mesh	PDMS			pressure sensing	125
coaxial	2D mesh	PDMS, PTFE		graphene	self-powered sensor	126
coaxial	2D pattern	Carbopol, silicone elastomers		Pt powder	microfluidics	127
coaxial	2D pattern	SF	water	CNT	TENG	128
coaxial	2D pattern	PVA	water	V_2O_5, MWCNT	supercapacitor	121
coaxial	2D pattern	HUVECs, VdECM, alginate, Pluronic F127			in vitro vascular models	129
coaxial	2D/3D pattern	TPU, PVA, PEO	DMF/water	ZnS, Ag, LiCl	stretchable electroluminescent device	118
coaxial	3D scaffold	PDA, alginate	Tris-HCl/ water		drug delivery	108
coaxial	3D scaffold	GelMA, alginate	water, HEPES, FBS	$CaCl_2$	tissue engineering	130
coaxial	3D scaffold	PDMS			electromagnetic interference shielding	131
coaxial	3D scaffold	PDMS		carbon	wearable sensor	132
coaxial	3D scaffold	polyester	camphene	alumina	bone tissue engineering	133
coaxial	3D scaffold	CMC, PCL	water	graphite, TCB	bone tissue engineering	134
coaxial	3D structure	ecoflex silicone		FS	actuator	135
coaxial	3D structure	PVDF	PC	CB	supercapacitor	122
coaxial	3D structure	PEG, GG	water	SiC, CF	mechanical reinforcement	136
porous	3D scaffold	PGS	ethanol	CNT	TENG	137
layer-by-layer	3D scaffold	SA	water	graphite	tissue engineering	138
layer-by-layer	3D structure	GelMA, alginate	FBS	nanosilicate, HAp	tissue engineering	139
layer-by-layer	3D scaffold	GelMA, alginate	DPBS		tissue engineering	140
segmented	single filament	rGO-poly(AMPS-*co*-AAm), silicon rubber	Tris-HCl	thermochromic microcapsules	dual parameter sensing	124
segmented	3D structure	epoxy, silicone elastomer			soft robotics	123
uniform	2D kirigami pattern	P(VDF-TrFE)	DMF	$BaTiO_3$, Ag	piezoelectric nanognerator	141
uniform	2D honeycomb pattern	gellan gum	water	PTFE nanoparticle	mechanical reinforcement	142
uniform	2D honeycomb pattern	PCE	water	nanoclay	mechanical reinforcement	143
uniform	2D interdigital pattern	ethyl cellulose, PVA	ethanol, water	CNT	microsupercapacitor	144
uniform	3D interdigital pattern		water	MXene	supercapacitor	145
uniform	2D auxetic pattern	ANF	DMSO		hydrophobic, luminescent and thermoresponsive architectures	146
uniform	2D mesh	dPVDF, PVP	DMAc		microfiltration	147
uniform	2D mesh	cellulose	EA		water/oil separation	148
uniform	3D scaffold	SA, cellulose	water		dye absorption	149
uniform	3D structure	PEG, GG	water	laponite, graphite	mechanical reinforcement	150
uniform	3D structure	PVA, PAM, PNIPAM, SA,	water		biomimicry organs	151
uniform	3D scaffold	epoxy		titanium powder	bone tissue engineering	152
uniform	3D scaffold	Pluronic F127	water	Bioactive 6P53B glass	bone tissue engineering	153
uniform	3D helical	GelMA	PBS		cell migration study	154

[a]ANF, aramid nanofiber; CB, carbon black; CF, carbon fiber; CMC, carboxymethyl cellulose; DMAc, *N*,*N*-dimethylacetamide; DMF, *N*,*N*-dimethylformamide; DPBS; Dulbecco's phosphate-buffered saline; DMSO, dimethyl sulfoxide; dPVDF, dehydrofluorinated PVDF; EA, ethyl acetate; EGaIn, eutectic gallium−indium; FBS, fetal bovine serum; FS, fumed silica; GelMA, myoblast-laden gelatin methacryloyl; GG, guar gum; Hap, hydroxyapatite; HEPES, 2-[4-(2-hydroxyethyl)piperazin-1-yl]ethanesulfonic acid; HUVECs, human umbilical vein endothelial cells; LFX, levofloxacin; LM, liquid metal; MWCNT, multiwalled carbon nanotubes; PAM, polyacrylamide; PBS, phosphate-buffered saline; PC, propylene carbonate; PCE, polycarboxylate ether; PCL, polycaprolactone; PDA, polydopamine; PDMS, poly(dimethylsiloxane); PEG, poly(ethylene glycol); PEO, poly(ethylene oxide); PGS, poly(glycerol sebacate); PI, polyimide; PNIPAM, poly(*N*-isopropylacrylamide); PTFE, poly(tetrafluoroethylene); PVA, poly(vinyl alcohol); PVDF, poly(vinylidene fluoride); P(VDF-TrFE), poly(vinylidene fluoride-*co*-trifluoroethylene); PVP, poly(vinylpyrrolidone); rGO-poly(AMPS-*co*-AAm), reduced-graphene-oxide-doped poly(2-acrylamido-2-methyl-1-propanesulfonic acid-*co*-acrylamide; SA, sodium alginate; SF, silk fibroin; TCB, β-tricalcium phosphate; TPU, thermoplastic polyurethane; VdECM, vascular-tissue-derived extracellular matrix.

result in specific structures on ice crystal templates. The freeze-drying combination with extrusion-based fiber spinning or DIW has also been recently developed for pore foaming or nanoparticle alignment. For example, Bai's group demon-

https://doi.org/10.1021/acsanm.1c01408
ACS Appl. Nano Mater. 2021, 4, 7538−7562

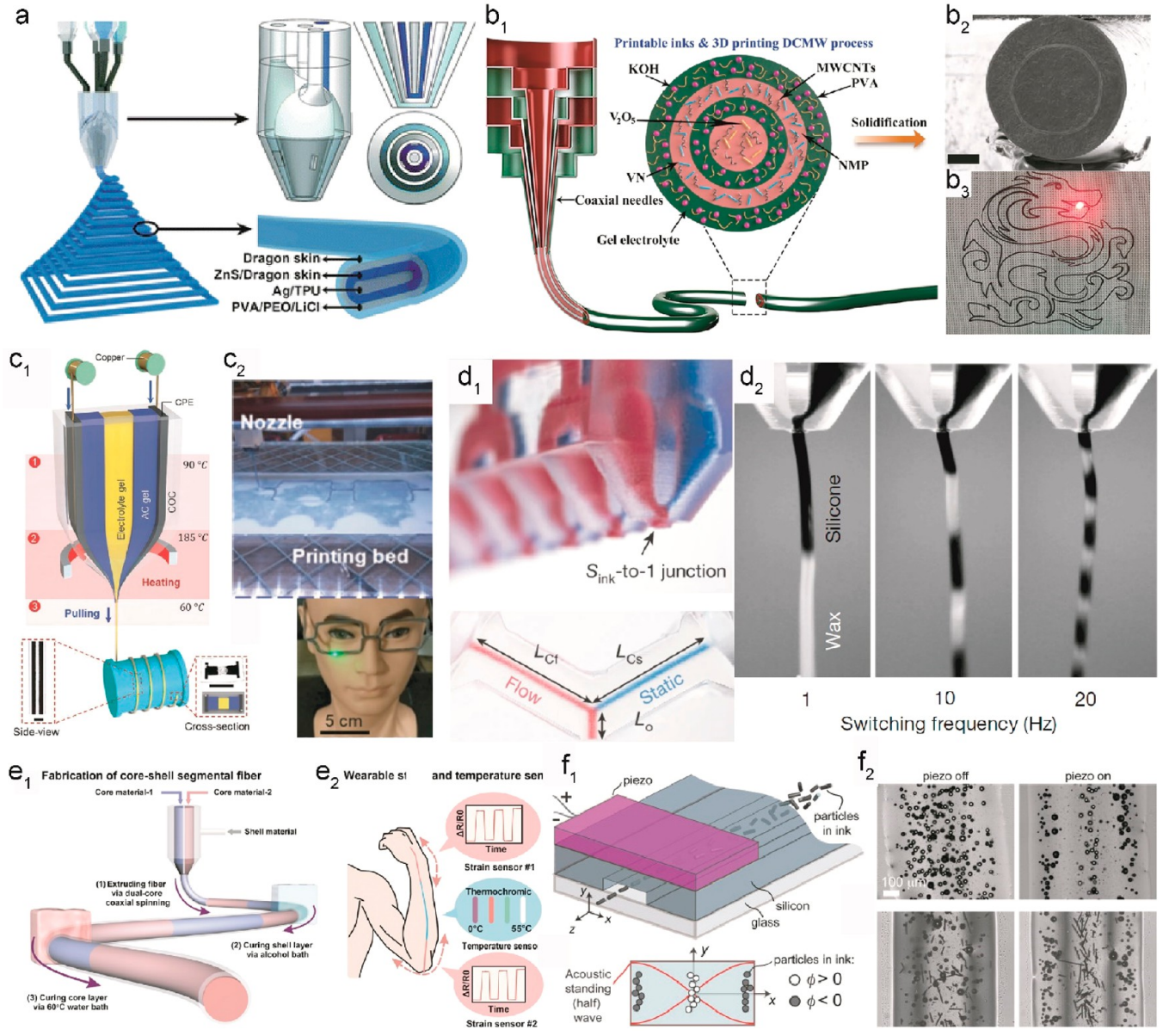

Figure 4. Microscale fiber structure features during DIW. (a) Multicore−shell printheads and printed 1D stretchable ACEL fiber devices. Reproduced with permission from ref 118. Copyright 2020 Royal Society of Chemistry. (b_1) Multicore−shell structure for a flexible supercapacitor through DCMW. (b_2) Cross-sectional SEM images of the fiber (scale bar: 100 μm). (b_3) Pattern demonstration of the fully charged supercapacitor with the lighting of a 1.5 V light-emitting diode. Reproduced with permission from ref 121. Copyright 2021 AAAS. (c_1) Fiber spinning of a continuous fiber supercapacitor as filament-based 3D printing. (c_2) Printing with supercapacitor fiber for energy applications. Reproduced with permission from ref 122. Copyright 2020 Wiley-VCH. (d_1) Two-material printhead with a cross-sectional view. (d_2) Two-material filament printing with an increase in the frequency for controlled material alternations within the same printing path (e.g., silicone and wax composition and order variations). Reproduced with permission from ref 123. Copyright 2019 Nature Springer. (e_1) Schematic illustration of the fabrication process for segmented core−shell hydrogel/thermochromic fibers. (e_2) Application demonstration of the segmented fiber for both strain and temperature parameter sensing. Reproduced with permission from ref 124. Copyright 2020 American Chemical Society. (f_1) Schematic of a microfluidic print nozzle coupled with a piezoelectric actuator excited at a frequency corresponding to a half-standing wave in pressure in the fluid. (f_2) Examples of particle separations. Reproduced with permission from ref 155. Copyright 2016 Elsevier.

strated a controllable growth of aligned pores during fiber spinning by introducing a cold copper ring. As the spinning dope slowly passed the ring, ice crystals grew directionally within the fiber, resulting in an aligned solute and pores (Figure 3e_1).[106] After the fiber was collected and freeze-dried, continuous and anisotropically oriented pores were formed within the fiber as a scalable thermal insulation material (Figure 3e_2).[106] A similar alignment effect was observed for DIW of GO for flexible supercapacitors by Song's group.[107] Neat GO was dispersed in water and extruded through a stainless steel nozzle of 200 μm diameter on a polyimide film. Afterward, the printed structure was freeze-dried for 12 h, followed by hydrazine hydrate reduction (Figure 3f_1). As the printed structure froze, the GO sheets were forced to align along the growing boundaries of the ice crystals. The eventual evaporation of ice into gas will retain this aligned GO morphology, forming a cellular network that addressed the limited areal capacitance of in-plane devices (Figure 3f_2).[107]

https://doi.org/10.1021/acsanm.1c01408
ACS Appl. Nano Mater. 2021, 4, 7538−7562

4. MICROSCALE FIBER STRUCTURES

On top of broad material choices and unique nanoparticle alignment, DIW of a fibrous structure also attracts researchers because of its versatile microscale fiber structures. Polymer/nanoparticle composite fiber has been a research focus for more than a few decades. In terms of material processing in conventional manufacturing, direct mixing of the polymer matrix and nanoparticle fillers for composites is often the solution for enhanced properties. The inclusion of DIW has made many complex microstructural designs feasible within the 1D fiber geometry. At the same time, fibers can form an assembly as textiles and system-level devices. A summary of recent DIW-based fiber materials is listed in Table 1 with diverse coaxial, layer-by-layer, segmented, and uniform fiber structures.

4.1. Multimaterial Fiber Structure. The coaxial layered structure has been a widely used fiber geometry for applications in biomedical materials,[108−110] drug delivery,[111,112] strain sensors,[113,114] and energy devices.[6,115,116] Unique material properties and applications are available by combining different material layers. Conventional fabrication methods for such a coaxial 1D fibrous structure usually involve layer-by-layer techniques. The complication for such discrete methods involves sophisticated steps and limitations by the overall integrity of manufacturing instruments. For instance, a 1D alternating-current electroluminescent (ACEL) fiber usually counts on a few processing steps to obtain the concentrically layered structure: a conductive coating-based inner electrode, a spray-coated or dip-coated phosphor layer of ZnS/elastomer, an outer electrode wrapped with conductive nanomaterials, and finally an encapsulation layer for practical applications.[117] Recent work by Zhou's group demonstrated a one-step fabrication process of multimaterial with a DIW technique for patterned optoelectronics with locally tunable light emissions (Figure 4a).[118] The 1D ACEL fiber consists of a phosphor layer with a ZnS microparticle with a dragon skin (DS) stretchable composite, silver/thermoplastic polyurethane (TPU) ink and ionic conductive gel as the two electrodes, and a transparent encapsulation layer DS outer layer with high stretchability. All layers are printed simultaneously after tuning of each layer's rheological behavior. The final 3D structure exhibits each layer's functionality, combining light-emitting and flexibility up to 450% deformation (Figure 4a).[118]

In contrast to traditional rigid energy storage devices, a fibrous supercapacitor has the advantages of excellent knittability, splendid flexibility, and high mechanical stability. The necessary electrodes, separators, and electrolytes make their fabrication process often too tedious and challenging to be cost-efficient.[119,120] Recently, Chen's group published their work using direct coherent multi-ink writing (DCMW) for coaxial patterned fibers as asymmetric supercapacitors (Figure 4b).[121] The smaller distance between the electrodes benefits electron transfer and ion diffusion within the electrode, thus showing superior performances compared to parallel and twisted fiber structures. Furthermore, the lower volumetric capacitance of the parallel structure prohibits its large-scale integration potential, while the unstable dynamic distance between the electrodes for the twisted structure deteriorates the electrochemical performance. Compared to the one-step printing procedure, the traditional layer-by-layer fabrication method for a coaxial structure suffers delamination problems under intensive bending mainly because of the loose interface contact between each layer during the multistep coating process. By utilizing a multichannel spinneret, Chen's group showed a promising method to generate a four-layered structure, with a diameter of 400 μm, in a single manufacturing step with enhanced interfacial interaction (Figure 4b$_1$).[121] When further combined with a 3D printing technique, DIW printed various battery shapes, demonstrating the versatile applications that benefited from high flexibility (Figure 4b$_2$).[121]

Fink's group also demonstrated a similarly all-printed supercapacitor consisting of four components, i.e., a porous electrode, electrolyte gels, a conductive polymer, and a copper current collector (Figure 4c$_1$).[122] A significant challenge in such a fiber structure is the incompatibility of the metallic current collector and polymer/ceramic electrode. This is resolved by intentionally incorporating the metal wires in a larger-sized hole within the polymer during a preform stage. After the fiber is thermally drawn, the gap gradually shrinks, and this eventually leads to a fully converged current collector and electrodes. The resulting fiber shows an energy density of 306 μWh cm^{-2} at 3 V and close to a 100% retention rate over 13000 cycles at 1.6 V. In addition, the fiber has excellent flexibility (5 mm radius of curvature), moisture resistance (100 washing cycles), and high strength (68 MPa). The fibers subsequently used as filaments for 3D printing demonstrated a 100% supercapacitor fiber-based eyeglass frame (Figure 4c$_2$).[122]

Apart from the core−shell structure where two or more materials lie parallel to the concentric direction, segmented fibers have also been processable for the multimaterial DIW process. By alternating the injection pressure at the nozzle, Lewis's group demonstrated voxelated material printing through DIW (Figure 4d$_1$).[123] The diode-like nozzle enabled high-frequency switching between up to eight different materials. Figure 4d$_2$ shows the DIW process of alternating wax and silicone at an increasing frequency. The precise control of multimaterial printing in a single step showed vast potential in origami and soft robotic printing with multimaterial-induced anisotropic mechanical properties.[123] Dong and others also demonstrated a segmented fiber structure with alternating conductive hydrogel and thermochromic elastomer (Figure 4e$_1$).[124] The hydrogel section showed strain sensing behavior, while the thermochromic section showed temperature-dependent color variations (Figure 4e$_2$). On top of this, their work also included a shell layer simultaneously extruded for maintaining the core fibrous shape as well as inhabiting hydrogel water loss, showing immense potential as wearable sensors (Figure 4e$_2$).[124]

The fiber's microstructure also includes different nanoparticle orientation patterns or distributions. External fields (e.g., electrical,[156,157] acoustic,[158] and magnetic fields[159]) have been efficient in nanoparticle configuration control in many 3D printing techniques. For example, Begley et al. showed that, by applying acoustic waves, different nanoparticles would reconfigure themselves based on either (i) an acoustic radiation force that acts to focus the particles to the center of the channel or (ii) secondary acoustic scattering forces that act to repel particles in the direction of wave propagation (Figure 4f$_1$).[155] As a demonstration, when hollow and solid spheres are printed, the solid spheres have a higher tendency of moving to the edge, while the hollow spheres are more likely to gather in the center of the printed line (Figure 4f$_2$). Such control over nanoparticle patterning inside printed fibers promotes enhanced nanoparticle loading without jamming and

https://doi.org/10.1021/acsanm.1c01408
ACS Appl. Nano Mater. 2021, 4, 7538−7562

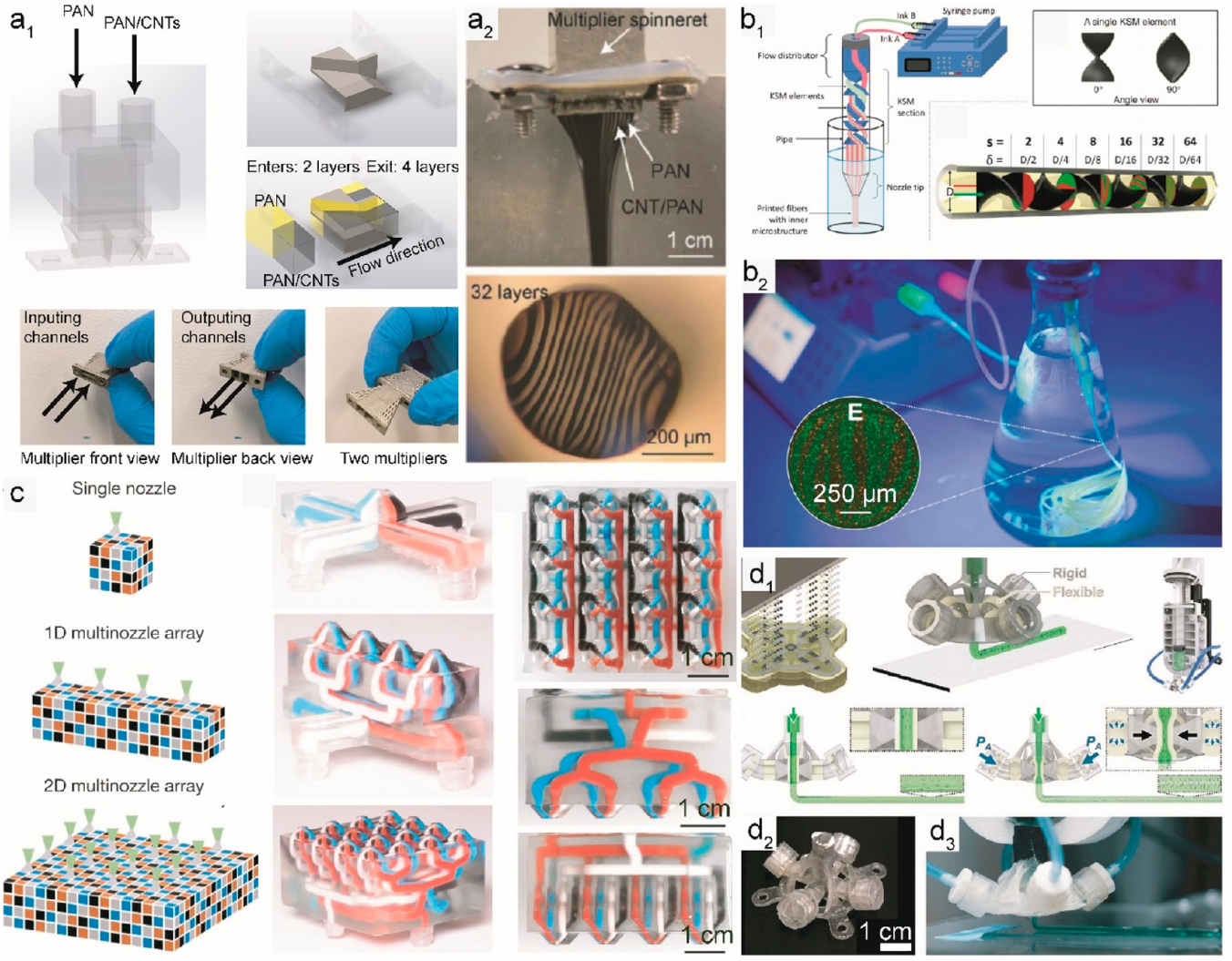

Figure 5. 3D-printed printheads for complex fiber structure. (a_1) Design and printed multiplication spinneret based on a metal SLS method for layer-structured fiber spinning. (a_2) Photograph of the air gap and optical cross-sectional image of a 32-layered fiber during fiber spinning. Reproduced with permission from ref 164. Copyright 2021 Wiley-VCH. (b_1) Experimental setup of chaotic printing for a multilayered structure with DLP-printed KSM. (b_2) Printed lamellar structure. Reproduced with permission from ref 138. Copyright 2020 IOP Publishing. (c) SLA-printed multimaterial printheads for 0D, 1D, and 2D DIW. Reproduced with permission from ref 123. Copyright 2019 Nature Springer. (d_1) Illustration of the PolyJet 3D printing process for the nozzle with its morphing mechanism. Microdroplets corresponding to flexible (black), rigid (white), and water-soluble (yellow) support materials. (d_2) Morphing nozzle after removal of the support material and (d_3) extrusion process. Reproduced with permission from ref 177. Copyright 2021 Wiley-VCH.

facilitated desirable nanoparticle distributions, eventually leading to enhanced mechanical performances.

4.2. 3D-Printed Spinneret for Innovative Fiber Structures. It is a clear trend that such 3D printing methods as single-step fabrication techniques toward multimaterial and hierarchical microstructures have grown tremendously. The innovation of 3D printing mechanisms and advancement of 3D printing precision are the primary driving forces toward this research trend. Many manufacturing opportunities limited by experimental setups are now open because of the marketization of 3D printing; researchers can design and rapidly prototype their printhead (i.e., spinneret) with highly customizable dimensions.

Metals are highly inactive to most organic solvents, polymers, or nanoparticles without acidic and basic solutions, making them ideal candidates for DIW printing nozzles. For instance, a SLS-printed coaxial spinneret from metals has been helpful for tissue scaffold,[160] drug delivery,[161] flexible electronics,[63] structural systems,[162] and volatile organic solvent (VOS) sensing applications.[163] Recently, Song's group applied metal SLS 3D printing with the traditional forced assembly process to generate alternating layered fiber structure with nanoscale CNT patterning (Figure 5a).[164] The forced assembly process has existed for a few decades; however, this processing has been in traditional use for multilayered polymer composite films as gas barriers and optical reflectors.[165−167] Because of its complicated experimental setup and sophisticated internal structure, its potential has not been expanded to other applications. In Song's work, as the two-channel solutions [i.e., polyacrylonitrile (PAN) and PAN/CNTs] first entered the 3D-printed multiplier, they were cut horizontally and rearranged vertically. As a result of this rearrangement, the two layers entering the spinneret would result in four layers exiting the spinneret (Figure 5a_1).[164] The spinneret dimensions were customized to match the viscoelastic behavior of the spinning solution to ensure lamellae flow during layer

https://doi.org/10.1021/acsanm.1c01408
ACS Appl. Nano Mater. 2021, 4, 7538−7562

formation at a nanoscale resolution. Figure 5a$_2$ shows the fabrication process of a 32-layered fiber. Likewise, the 512-layered fiber eventually obtained had a layer thickness down to 170 nm. Such a nanoscale patterning of CNTs resulted in enhanced nanoparticle dispersion and orientation, leading to superior mechanical properties compared to fibers without layered structure. The same group also demonstrated using the same spinneret in the DIW 3D printing process for thin films and patterns with enhanced mechanical properties. With a rectangular-shaped exit, the DIW printhead can deposit composites with layered structures within an individual printing line. The layers are composed of poly(vinyl alcohol) (PVA) and PVA/CNT content similar to the layered structures in Figure 5a, showing incrementally increased modulus and strength with a decrease of the layer thickness.[168]

Compared to metal SLS, light-initiator-based 3D printing usually incorporates monomer-based resins more susceptible to solvents and should have cautious applications. On the other hand, their higher printing resolution could produce more intricate features. For example, a static mixer is a device made of a series of valves that control the flow of pressure-driven liquids and has wide applications in various industries, ranging from polymer processing and biotechnology to water treatment.[169] Similar to the forced assembly process, the intricate internal structure design and the large scale of such devices limited most academic researches to numerical analysis or simulation of the dynamic flow for industrial applications.[170,171] Recently, the Khademhosseini, Alvarez, and Santiago groups replicated the kinetic static mixer (KSM) for biological applications using a DLP 3D printer.[138,140,172] With the high printing resolution, laboratory-scale KSM was achieved. The resulting alternating layers of inks A and B showed the lowest layer resolution of 10 μm for DIW and 150 nm for electrospinning (Figure 5b$_{1-2}$).[138] Furthermore, such a well-defined internal multilayer microarchitecture has a high throughput of >1 m min^{-1}. Together, the printed scaffold structure demonstrated novel applications, including, but not limited to, bacterial communities, living tissues composed of organized multiple mammalian cell types, and the fabrication of smart multimaterial and multilayered constructs for biomedical applications.[138] SLA is the general photoinitiator-based 3D printing technique that has been used frequently for achieving complex experimental setups.[173−175] For instance, Lewis and others demonstrated their multimaterial multinozzle 3D (MM3D) printing technique based on a SLA-printed spinneret.[123] These MM3D printheads can deposit up to eight materials, each of which flows through independent bifurcating channel networks that reside within the printhead (Figure 5c).[123] By control of the pneumatic solenoids, different pressure flows were applied to each channel, achieving manageable material switching at high frequency.

Inkjet-based 3D printing, such as PolyJet, is another method for 3D printing with acceptable resolutions, multimateiral compatibility, and structural complexity that traditional machining or molding cannot achieve. Its unique advantage of incorporating different materials into a single model has shown increasing interest in tooling engineering.[176] Recently, Sochol's group utilized PolyJet printing to construct a shape-changing spinneret for nanoparticle orientation control.[177] Flexible, rigid, and water-soluble parts were printed at once (Figure 5d$_{1-3}$).[177] After washing away the water-soluble part (Figure 5d$_2$), the rigid and compliant materials enabled manipulation over the internal extrusion channel through pneumatic inputs (Figure 5d$_1$).[177] Conventionally, nanoparticles are in favor of alignment in the printing direction. By changing the straight extrusion channel to a converging-diverging configuration, the corresponding carbon microfiber also, in turn, experienced a transition regarding their orientation; instead of the conventional anisotropic swelling behavior, the reduced alignment promoted isotropic water-induced swelling properties.[177]

5. MACROSCALE FIBER PATTERNING

Combining the traditional fiber spinning technique with an XYZ linear stage on a 3D printing platform can achieve a higher degree of control over spinning parameters, including extrusion speeds, printhead travel rates, solidification periods, and air-gap distances. For instance, the coagulation period is critical for fibril structural formation that can vary from a few seconds (e.g., for DMF/PAN in water coagulants)[164] to tens of minutes [e.g., for dimethyl sulfoxide (DMSO)/TPU in methanol coagulants][163] depending on the solvent/polymer system and their thermodynamic interactions with nonsolvent coagulants. Patterning the as-spun fibers inside the limited coagulation bath is a viable strategy for such slow coagulating materials. Furthermore, the versatile fabrication process of DIW makes printing feasible on different substrates without additional pattern transfer steps as stamping or sacrificial layers.[178,179] Substrate types, like metals,[180,181] paper,[182,183] ceramics,[184−186] fabrics,[187−190] and polymers,[191−195] are selected based on the desired applications. For example, soft polymer substrates are often considered for wearable electronics because of their flexibility and comfort.[196−201] Zhang's group demonstrated the direct printing and patterning of a core−shell-structured E-textile on conventional fabrics.[128] The adhesion between the E-textile and substrate was firm, resulting in a stable voltage output over 15000 cycles of loading and unloading, and resistant to peeling using standard adhesive tapes. With SF as the dielectric shell and CNTs as the conductive core, the pattern E-textile was used directly on cloth as a wearable triboelectric nanogenerator (TENG) capable of harvesting electricity from human motion and achieved a high power density of 18 mW m^{-2}.

Last but not least, in contrast to traditional textile engineering, where 1D fibers are collected and assembled into 2D or 3D structures via knitting or weaving, 3D printing techniques offer unique integration platforms with high structural designability and manufacturing customizability. Therefore, in this section, different types of fiber patterning will be the discussion focus, with the 2D/3D structural characteristics highlighted for broad applications. A summary of recent DIW-based fabric materials and devices is given in Table 1 with 2D/3D patterned architectures, and the reported applications primarily focus on (i) intelligent materials (e.g., sensors, actuators, and soft robotics), (ii) energy generations and storage [e.g., supercapacitors, batteries, TENGs, and piezoelectric nanogenerators (PENGs)], and (iii) biomedical applications (e.g., tissue scaffolds and drug delivery).

5.1. DIW-Enabled 2D Patterning. Although fabrics look similar macroscopically, they consist of different sewing techniques, such as knitting, braiding, weaving, and non-woven.[202,203] Within each sewing category, different types of interlacements separate one from another. Similarly, in DIW, various strategies can arrange 1D fibers as fundamental building blocks into 2D patterns. Unlike fabric sewing, where the same patterns are repeated in high density to achieve

https://doi.org/10.1021/acsanm.1c01408
ACS Appl. Nano Mater. 2021, 4, 7538−7562

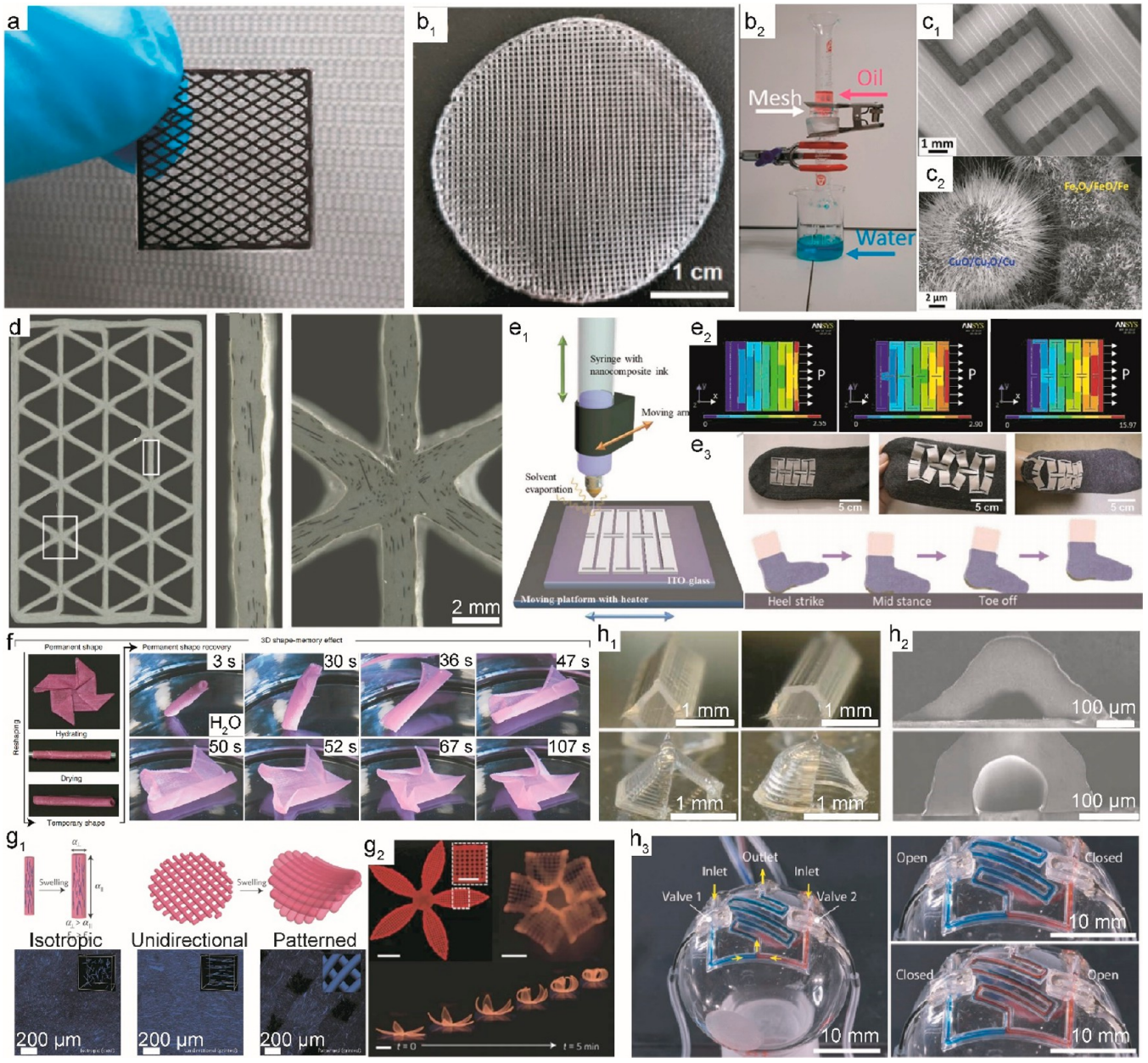

Figure 6. 2D patterning in DIW. (a) Printed GPN with a controllable pattern. Reproduced with permission from ref 209. Copyright 2020 American Chemical Society. (b_1) Digital images of 3D-printed cellulose acetate meshes for (b_2) oil−water separation. Reproduced with permission from ref 148. Copyright 2019 American Chemical Society. (c_1) SEM micrograph of the sensor element with interdigitated patterns. (c_2) SEM image of the nanospikes between Cu−Fe microparticles. Reproduced with permission from ref 186. Copyright 2020 Elsevier. (d) Optical images of triangular honeycomb structures with SiC-filled epoxy and a zoomed-in section showing the Si−C alignment. Reproduced with permission from ref 222. Copyright 2014 Wiley-VCH. (e_1) Fabrication process of a PENG (e_2) showing FEM simulation of simple, fractal-cut, and T-joint-cut kirigami structures. (e_3) Actual printed structure on socks showing different movements for generating voltage responses. Reproduced with permission from ref 141. Copyright 2020 Elsevier. (f) DIW of keratin fiber fabric with shape-memory properties in response to hydration. Reproduced with permission from ref 230. Copyright 2021 Nature Springer. (g_1) Isotropic (cast), unidirectional (printed), and patterned (printed) cellulose fibrils during hydrogel DIW for anisotropic swelling behavior. (g_2) Demonstration of biomimetic 4D printing of a flower pattern. Scale bars: 5 mm; (inset) 2.5 mm. Reproduced with permission from ref 238. Copyright 2016 Nature Springer. (h_1) Photograph of a cross section of the self-supporting structure. (h_2) SEM images of triangular and circular channels. (h_3) DIW of patterned microfluidic channels on a spherical surface with integrated valves. Reproduced with permission from ref 239. Copyright 2020 AAAS.

mechanical stability and cost efficiency, the flexible customization of DIW offers high control over the position and configuration of each fiber for precise manipulation of the pattern density, pattern direction, and structural-induced functionalities. In this section, we will discuss the DIW-enabled 2D patterning used for lightweight composites (e.g., cellular systems and kirigami structures), intelligent systems [e.g., sensors, batteries, actuators, and thermoelectric (TE) devices], and sustainability (e.g., membranes for filtration and water purification).

Mimicking the mesh pattern in traditional fabric materials for mechanical flexibility, durability, and comfort is common in 3D printing approaches. By the direct incorporation of functional nanoparticles inside each fiber building block, the

https://doi.org/10.1021/acsanm.1c01408
ACS Appl. Nano Mater. 2021, 4, 7538−7562

integrated devices can serve as wearable electronics,[204] sensors,[205] environmental applications,[147,149] tissue supports,[206] and thermally regulated textiles.[207,208] For example, Dong's group demonstrated a graphene-based planar network (GPN) through DIW with different ribbon packing densities and oblique angle directions that ensured mechanical stability during deformation and, at the same time, showed better sensitivity compared to a traditional woven fabric coated with a graphene layer (Figure 6a).[209]

A similar mesh structure with controlled pores and hydrophobicity or hydrophilicity can help the water−oil separation. For example, He et al. demonstrated the printing of a superhydrophilic mesh structure from cellulose acetate/ethyl acetate. With a pore size smaller than 280 μm, the mesh's separation efficiency achieved over 95% (Figure 6b$_{1-2}$).[148] When the pattern was tailored from a simple square shape to a quad-layer structure, the efficiency further improved to 99% (Figure 6b$_1$).[148] The 3D-printed cellulose structure also showed higher stability than traditional cellulose-coated fabrics, where coating inhomogeneity and poor interfacial adhesion have been problematic.

The interdigital circuit has broad applications as conductive electrodes with metal or semiconducting materials processed in traditional masked lithography.[210] As a comparison, DIW offers a broader range of materials and can accommodate the printing of interdigital circuit patterns for energy storage systems,[33,144,211−213] bioelectrodes,[214,215] and sensing applications.[186,216] For example, Lewis's group demonstrated an all-DIW-printed battery with an interdigital circuit structure, from the gold current collector to $Li_4Ti_5O_{12}$ and $LiFePO_4$ electrodes.[212] Furthermore, DIW also offers a nanoscale hierarchy structure that generally is not accessible via conventional sputtering. For example, Adelung's group recently developed a highly sensitive acetone vapor monitoring device based on DIW-printed nanowires and nanospikes of $CuO/Cu_2O/Cu$ and Fe_2O_3/Fe heterojunctions (Figure 6c$_1$).[186] The rheologically optimized ink contained copper and iron microparticles as conductive media, poly(vinylbutyral) as the binder, and ethanol as the solvent. The microscale interdigital pattern had a height of 0.1 mm and a width of 0.6 mm after printing. At the nanoscale, the spikelike structure between copper and iron oxide within each printed line increased the active surface area, facilitating easier gas diffusion and ultimately leading to the fast detection of various VOSs at low concentrations (Figure 6c$_2$).[186]

Patterns with unique cellular structures are well-known for exceptional mechanical reinforcement, stretchability, and tunable Poisson's ratios.[217−220] For example, the honeycomb structure will experience three steps under compression. The first regime is the linear elastic regime, where the cell walls bend. The second regime is the stress plateau, during which buckling, yielding, and brittle crushing happen. Finally, it is densification, where the cell walls touch each other. Under tension, the first regime is also linear elastic, corresponding to cell wall bending. If the cell walls yield, there will be a stress plateau. With brittle cellular walls, the honeycomb will fracture under tension. A detailed analysis is explained elsewhere.[221] Specific out-of-plane properties are also required because honeycombs are usually used as cores in sandwich structures and energy absorbers from impact. DIW with parametrized g-code scripts allows the generation of such complex geometries for various applications. For example, by mimicking the general honeycomb structure, Lewis's group developed a 3D-printed lightweight epoxy composite with nanoclay platelets as a rheological modifier, dimethylmethyl phosphonate as a viscosity reducer, and silicon carbide (SiC) as a reinforcement filler (Figure 6d$_1$).[222] Because of the SiC whisker alignment and cellular structures, the printed material showed exceptional mechanical properties (Figure 6d$_2$).[222] In piezoelectric materials, the polymer−nanoparticle strain mismatch during mechanical cycling is often responsible for the overall response relaxation.

A kirigami structure, often obtained through a paper-cutting technique, can sustain up to 30% strain while retaining the optimum material composition used for flexible supercapacitors, solar cells, and strain sensors.[223−225] However, traditional paper-cutting patterns are often used for out-of-plane bending or tilting, making the structure unsuitable for pressing or compressing, which unfortunately would result in the highest piezoelectric constant for energy-harvesting devices. To solve this, Lee's group used the DIW technique to modify traditional kirigami structures by introducing T-joint-cut patterns to the $BaTiO_3$-nanoparticle-based PENG (Figure 6e$_1$).[141] Finite-element method (FEM) analysis confirms that the deformation under pressure was the greatest for the T-joint-cut patterns (Figure 6e$_2$).[141] When such printed patterns are applied on the bottom of socks, energy signals are generated with compression motions (Figure 6e$_3$).[141]

Shape-morphing fibers are also helpful in civil engineering,[226] aerospace,[227] wearable electronics,[228] and medical devices.[229] Their spatial geometry could be manipulated by applying different types of stimuli. 2D patterning of these 1D fibers plays a significant role in the overall device application.[230−234] For example, Parker's group recently developed a bioinspired and hierarchically structured shape-memory fiber with extracted keratin from angora wool. The shape-memory effect of such a fiber relies on the reversible uncoiling of the α-helix and the formation of metastable β-sheets when uniaxial strain is applied. Through DIW of the extracted protein dope into a hydrogel, which acted as both a coagulation bath and a supporting fluid, a shape-memory fiber was constructed into complex geometries. For a demonstration, water was used as the stimulus to perform the shape-recovery behavior of a star-shaped fabric (Figure 6f).[230] Another strategy for shape-morphing 2D materials is based on the patterning of different materials or material types during DIW.[123,235−237] For example, Agarwal's group showed a simple strategy of combining electrospun thermoresponsive poly(*N*-isopropylacrylamide) (PNIPAM) as the morphing substrate to DIW print and pattern PNIPAM/clay-based composites. The swelling mismatch between the substrate and printed pattern at different temperatures resulted in complex shape transitions.[235] Zhao's group also showed the development of a fast-transforming soft material from DIW through the controlled alignment of ferromagnetic microparticles during printing. The printed pattern with programmed ferromagnetic domains demonstrated complex shape changes under applied magnetic fields.[237] Similarly, Lewis et al. showed that different swelling behaviors could be preprogrammed through the patterning of each extruded fiber filament with anisotropic cellulose fibril alignment (Figure 6g$_{1-2}$).[238]

DIW also allows highly customized printing shapes not following conventional designs and only dependent on the device applications. For instance, pressure-mapping sensors on shoes are highly customized, considering the typical pressure concentrated on the metatarsal and heel bone during walking.

https://doi.org/10.1021/acsanm.1c01408
ACS Appl. Nano Mater. 2021, 4, 7538−7562

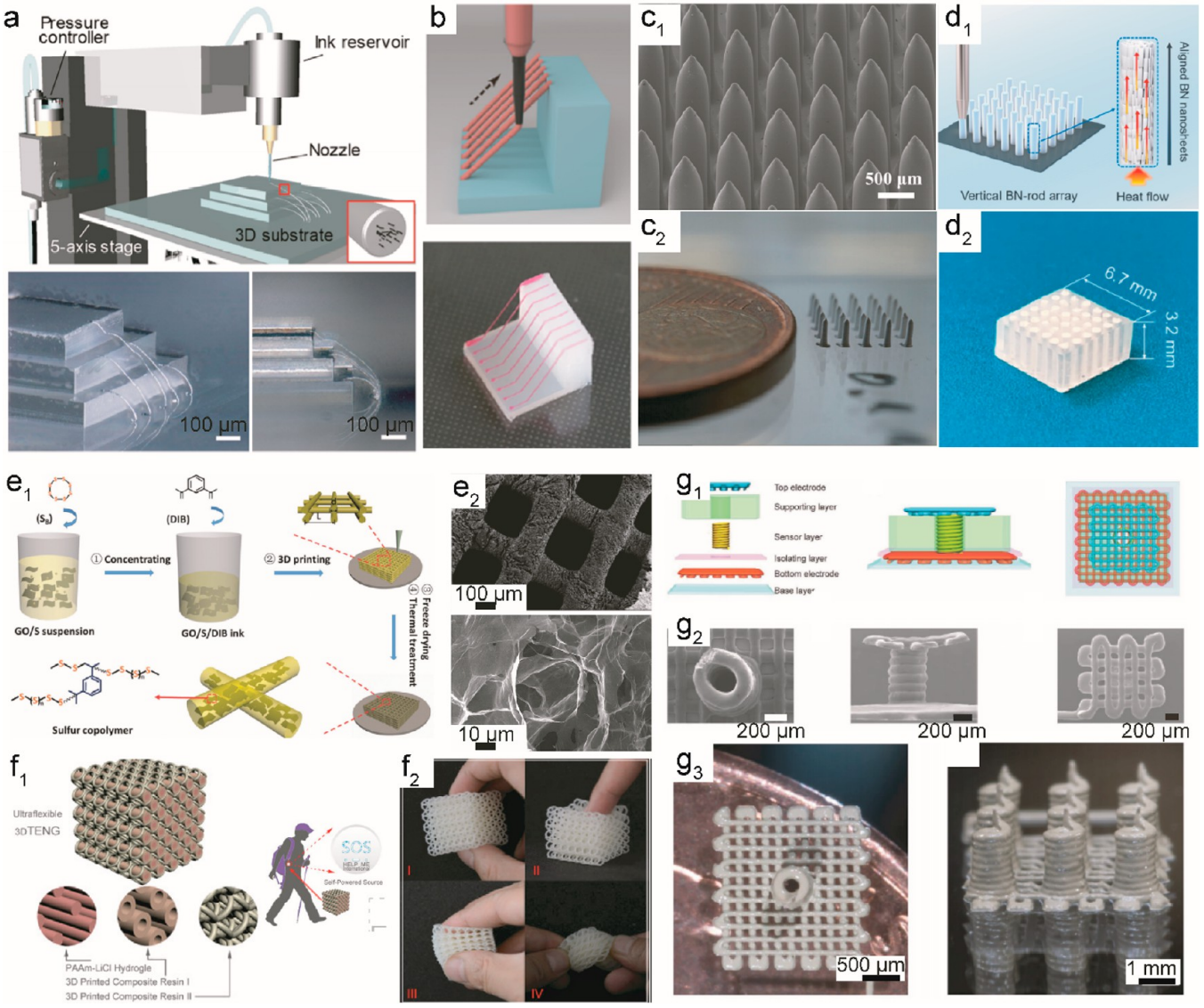

Figure 7. 3D patterning in DIW. (a) 3D printing of CNT/LM on microsteps for wiring applications. Reproduced with permission from ref 180. Copyright 2019 American Chemical Society. (b) Omnidirectional printing of self-supporting structures at a step angle of 60°. Reproduced with permission from ref 240. Copyright 2019 American Chemical Society. (c_1) SEM images of verticle zirconia pillars and (c_2) aluminum pillar arrays on glass. Reproduced with permission from ref 247. Copyright 2020 Elsevier. (d_1) Schematic showing vertical DIW of a BN array, with zoomed-in sections showing shear-induced BN nanoparticle alignment. (d_2) Six-by-six vertically aligned BN array in PDMS. Reproduced with permission from ref 244. Copyright 2019 American Chemical Society. (e_1) Schematic demonstration of 3D printing sulfur copolymer−graphene architectures. (e_2) SEM images of the printed electrode with macroscopic and microscopic pores. Reproduced with permission from ref 266. Copyright 2017 Wiley-VCH. (f_1) 3D structure of TENG from DIW of bulk/support material printing, with the inset demonstrating its wearability, and (f_2) flexibility test. Reproduced with permission from ref 275. Copyright 2018 Elsevier. (g_1) Schematic and (g_2) SEM images of the tactile sensor consisting of different layers 3D-printed from DIW. (g_3) Top view of a single sensor and side view of a tactile sensor array. Reproduced with permission from ref 274. Copyright 2017 Wiley-VCH.

As a result, the DIW-based devices have higher sensor array density in these places to maximize mapping resolution.[192] Another example is that, during the fabrication of TE devices, one challenge is to fit the TE materials perfectly to different heat sources. Son et al. demonstrated DIW printing of conformable Bi_2Te_3-based inks directly onto the surface of an alumina pipe for shape-optimized performances to address this issue.[43] Similarly, McAlpine's group also demonstrated DIW of a self-supporting microfluidic device on freeform surfaces with silicone-based ink. Different triangular or rectangular microchannels were printed by stacking each fiber without any supporting structure (Figure 6h_{1-2}).[239] Through DIW, these building blocks were further integrated into complete microfluidic networks and printed directly onto a spherical surface, demonstrating a previously unrealized device structure (Figure 6h_3).[239]

5.2. DIW-Enabled 3D Patterning. With multidirection nozzle movement capability, DIW of 1D fiber building blocks has achieved different 3D patterns that traditional fiber sewing could not easily make, despite the fact that fabrics combined with stacking techniques and polymer molding for 3D composites are standard in the aerospace and automobile industries. Different 3D patterns have been categorized into omnidirectional patterning, vertical patterning, 3D scaffold

https://doi.org/10.1021/acsanm.1c01408
ACS Appl. Nano Mater. 2021, 4, 7538−7562

patterning, and 3D functional device patterning, as summarized in this section.

One strategy to achieve omnidirectional printing is through self-supporting inks that are mechanically strong enough to overcome the gravitational force. For example, Park's group showed 3D printing of liquid metal (LM) of eutectic gallium−indium (EGaIn) and CNTs on stepped surfaces with heights ranging from 100 to 300 μm for wiring applications (Figure 7a). Similarly, Kong's group also demonstrated an omnidirectional DIW strategy by tuning the viscosity behavior of the ink by optimizing fumed silica. To show the high degree of freedom in the printing direction, they printed an array of noncoplanar filaments that bridged two surfaces at a considerable height difference at 60° (Figure 7b).[240] As briefly mentioned before, EMB3D is also a viable method for omnidirectional writing. Different from using high elastic inks in omnidirectional printing, the use of a supporting fluid in EMB3D is suitable for low-viscosity materials that can be useful to engineer biomimetic and dynamic tissuelike constructs.[241−243]

Properties in the vertical direction are crucial for many applications, from low tortuosity for rapid ion transport to aligned thermal pathways for electronics cooling. Despite 2D or 3D patterning, the DIW process usually utilizes a predesigned path in the $x-y$ direction with appropriate increments in the z axis. However, this process is highly inefficient for vertical features because the resolution of the printed pillar could seriously deteriorate if $x-y$ slicing was used. Therefore, many efforts have been made to develop vertical DIW patterns for heat sink,[244] cell culture,[245] electronics,[92] and surface plasmon resonance applications.[246] For example, Ferreira's group showed a guideline for single-pillar DIW that takes the printing speed/direction, end pressure, and ink's thixotropy properties into account.[247] For a demonstration, materials including zirconia, a lead-free $Ba_{0.85}Ca_{0.15}Zr_{0.1}Ti_{0.9}O_3$ piezoelectric material, and aluminum-based pillars were printed with large length-to-diameter ratios (Figure 7c_{1-2}). Hu's group also demonstrated vertical printing of the pillar structures with a high 2D BN nanoparticle loading. By extrusion of an optimized ink with high BN concertations, ultrahigh storage modulus, and shear-thinning behavior, BN pillars were printed vertically as thermal pathways with shear-induced BN platelet alignment, achieving a high vertical thermal conductivity of 5.65 W m^{-1} k^{-1} (Figure 7d_{1-2}).[244]

DIW of a cellular-structured material is one of its dominant applications. The main features of cellular solids include low weight, the ability to undergo large deformations, low thermal conductivity, and a large surface area. The cellular materials can be found in nature, for example, microstructures of trabecular bones,[248] cellular structures in wood,[249] forms in plant parenchyma,[250] and sandwich structures in bird skulls.[251] An extrusion process, casting, and a biocarbon template method are often used besides DIW.[252] Cellular solids could be 2D or 3D depending on whether the polygonal cells pack to fill the 2D plane (2D honeycombs as discussed previously) or the polyhedral cells pack to fill space (3D foams). The properties of the solid it is made from, the relative density and cell geometry, will influence their properties. For cellular solids, the typical relative density, which is the ratio of the density of a cellular solid and the density of the solid it made from, is less than 0.3. For example, the relative density of polymer foams is usually between 0.02 and 0.2.[253,254] If the relative density is larger than 0.8, the structure will become isolated pores in a solid. Besides, hexagons, triangles, and squares are also forms of unit cells of 2D honeycombs.[255] The unit cells can be stacked in more than one way. Rhombic dodecahedra and tetrakaidecahedra unit cells are frequently seen in 3D foams. Moreover, the cell shape, mean intercept length, and anisotropy of the unit cells have an impact on the solid.

Tissue engineering scaffolds can facilitate the regeneration of damaged tissues. It resembles the extracellular matrix that cells are attached to in the body. A large volume fraction of interconnected pores is needed for cell migration and nutrient transportation, making it cellular. Commonly used materials are natural polymers, such as collagen, chitosan, and alginate, synthetic biopolymers, such as poly(lactic acid), PCL, and polyglycolide, and hydrogels, such as PEG, PVA, and poly(acrylic acid). The material degradation rate, cell attachment, cell morphology, cell contractility, cell migration, and cell differentiation are usually evaluated for tissue scaffolds. For example, fabricating an osteochondral scaffold should mimic the mechanical properties and the structure with the gradient interface of the osteochondral tissues with well-tuned porosity, pore size, and mineral content.

Compared to other 3D patterning techniques (e.g., molding, colloidal templating, electrospinning, leaching, or interference lithography), the extrusion-based DIW method enables a flexible fabrication process with independent control over the extruded filament diameter, pitch, macroporosity, and material section tunable for specific applications. For example, the scaffold geometry (e.g., pore size and porosity) is a significant factor for the 3D scaffold performance in biomedical applications.[256−259] Shah's group printed two geometries with different strut angles, either 90° or 60°, between subsequent layers with gelatin for seeding hepatocytes. Although the two geometries did not show a significant difference in cell proliferation, the 60°-angled structure showed higher performance (i.e., albumin secretion, cytochrome P450 activity, and bile transport) because of higher interconnections in the gelatin scaffold.[260]

Another interest in 3D scaffold structures is their high surface-to-volume ratios, resulting from bottom-up stacking of high-aspect-ratio 1D filaments. This large aspect ratio of printed structures has been particularly interesting for energy-related applications because it offers a shorter ion pathway and higher interfacial reaction rates.[40,261−265] For example, Yang's group recently demonstrated a 3D-printed scaffold structure for a lithium−sulfur battery electrode by DIW of the sulfur copolymer and GO, followed by freeze-drying and thermal annealing (Figure 7e_1).[266] The printed scaffold consisted of both visible pores (about 300 × 300 μm) from DIW patterns and microscopic pores from randomly stacked 2D graphene flakes, which all contributed to a higher electrolyte penetration depth and a high reversible specific energy density, reaching up to 812.8 mAh g^{-1} (Figure 7e_2).[266]

DIW of an aerogel is another strategy often used to construct hierarchical structures across the nanoscale and macroscale.[267−269] Du's group demonstrated DIW of different types of aerogel-based inks, with the highest specific surface area reaching 613 m^2 g^{-1} for a resorcinol−formaldehyde aerogel.[270] Similar to multimaterial printing in 1D fibers or 2D surfaces, 3D scaffolds also benefit from using different materials to achieve multifunctional performances. For example, Wang's group demonstrated a 3D-printed TENG with both flexibility and the ability to harvest biomechanical energy (Figure 7f_{1-2}).[271] Through multimaterial printing of

https://doi.org/10.1021/acsanm.1c01408
ACS Appl. Nano Mater. 2021, 4, 7538−7562

sacrificial internal support and electrification materials, a complex 3D structure was obtained with high endurance to mechanical deformation. Through the assembly of ionic hydrogel electrodes into a predesigned location, a self-powered wearable TENG was developed with an output energy of 10.98 W m^{-3}.[271]

The high degree of freedom during 3D DIW usually results in innovative structures that are difficult to categorize. The design of these structures is highly dependent on the device application, such as soft robotics,[151] 3D sensors,[272] 3D organic prototyping,[268,273] or mechanical structures.[150] For example, McAlpine's group demonstrated 3D tactile sensors that can conformally attach onto freeform surfaces through multiple DIW procedures with various combinations of silver and silicone (Figure 7g_{1-2}).[274] The unique spring-structured sensing layer, together with large upper and lower electrodes, achieved a gauge factor of around 180 to compressing motion with high reversibility. The sensor was further scaled up into array structures for electronic skin applications to collect spatially resolved pressure information (Figure 7g_3).[274] These 3D-patterned structures have a primary driving force from specific applications, depending upon the proper material selections and requiring desirable printing resolutions.

6. CONCLUSION AND FUTURE PERSPECTIVES

A 1D fiber has been the building block for textiles and fabrics for centuries. However, the rapid development of 3D printing has recently challenged the concept of fiber spinning and textile engineering because of intrinsic features including design, fabrication, property optimization, tooling engineering, and manufacturing scalability. DIW-based 3D printing shares many similarities with fiber spinning, i.e., high compatibility to multimaterial composites or hybrids, low-viscosity processability, and flexibility with application-driven structures. Besides, the DIW method has superior technology transferability because of its user-friendly and straightforward extrusion characteristics, making it one of the most cost-efficient and low-footprint manufacturing techniques for making 1D fibers, 2D surface orders, and 3D layers.

This review paper has systematically discussed this trend of incorporating fiber-making capabilities in DIW printing methods with an overview of structural identity at the nanoscale, microscale, and macroscale. Looking at the nanoscale, the extrusion-induced and shear-facilitated nanoparticle alignment has enhanced mechanical and functional properties in DIW-printed nanocomposites. Focused at the microscale, the selective position of multiple materials concentrically or along the fiber axis (e.g., core−shell, segmented, and layer-by-layer coaxial stacking) enables multifunctional composites in which a single-composition or single-phase material is challenging to achieve. Consistent with the nanoscale particle alignment and microscale material placement, the highly tunable deposition of fibers via the DIW method presents one-step manufacturing for macroscale patterns. Moreover, unlike traditional fabrication techniques where device functions and properties are only dependent on the material section, DIW allows independent control over the printing pattern, direction, resolution, and speed, which opens up new pattern-based functions. In essence, the deposition of fibers in DIW incorporates top-down processing (i.e., from fiber to fiber-contained nanoparticle alignment) and bottom-up manufacturing (i.e., from fiber to fiber-stacked layers). The nanoscale particle alignment, microscale composition selectivity, and macroscale patterns in DIW naturally embrace a cross-scale hierarchy. Nevertheless, DIW suffers from several imperfections requiring multidisciplinary efforts before achieving its full potential and broad applications.

(1) First, DIW-printed products have limited material mechanics because of the softness and compliance of printing inks. The low mechanical robustness is one reason why DIW-enabled materials have limited and dominant applications in tissue scaffolds, stretchable electronics, and wearable energy generators. Although nanoparticles can enhance the mechanical properties, the use of a DIW feedstock in the form of nanoparticle colloids, polymer solutions, and gel-like composite mixtures makes it challenging to compete with conventional fiber materials, considering the possibility of postspinning treatment in improving the polymer crystallinity, molecular orientations, nanoparticle alignment, and their effects on fiber mechanics. Therefore, innovative approaches for increasing the mechanical properties are critical for DIW-printable objects in high-performance structural material or mechanically durable functional device applications.

(2) Second, because of the nozzle-based extrusion, the DIW method cannot generate a high printing resolution like many other AM platforms. For example, two-phonon or multiphoton polymerization can have a voxel size at ∼100 nm,[17] and EHD jetting efficiently produces a printing line of 65 nm.[18,276] Compared to these methods, DIW has the advantage of much higher manufacturing rates and material versatility, especially inks with a wide range of flow behaviors. However, its printing resolution is restrained by the size of the nozzle, typically ranging from 100 μm to 1 mm. To address this issue, printing techniques such as deformation printing,[277] which harnesses the deformation, instability, and fracture of viscoelastic ink, or meniscus-guided printing[91,278,279] have recently been investigated for production of a resolution much smaller than the nozzle size. Other efforts beyond manipulation of the material characteristics (e.g., multiphase printhead design or microfluidic innovation in extrusion) may significantly transform the printing resolutions and broaden DIW-enabled applications.

(3) Third, low-loading nanoparticle-based suspensions have too low viscosity and viscoelasticity to print, and higher concentrations may clog the printhead, justifying the use of polymers to assist in continuous and smooth printing. However, in the printing of any nanoparticle-based material, such as battery electrodes and thermal pathways, the use of polymer binders always deteriorates the electron, phonon, or ion transport capabilities, resulting in an inferior performance compared to material-filled methods. To address such an issue, researchers will need to develop inks with proper nanoparticle loading for achieving adequate flowability, low binder concentration, or postprinting treatment to eliminate polymers for a highly desired functional performance.

(4) Last but not least, another problem with DIW is its scalability potential for industrial applications. SLS/SLM for metal parts has found practical aerospace or energy systems (e.g., old engine parts and wind turbine components), as evidenced by the collaboration between 3D systems or Stratasys with defense stakeholders. The continuous liquid interphase printing technique has demonstrated 100 times faster printing speed than general SLA, attracting business from automotive, dental, and life sciences.[280] A similar extrusion-based FDM has also seen success among amateur players because of its standard feedstock, user-friendliness, and low

https://doi.org/10.1021/acsanm.1c01408
ACS Appl. Nano Mater. 2021, 4, 7538−7562

printer cost. Thus, more attention should be given to DIW standardization, cost efficiency, and broader applications.

In summary, looking back at DIW with its single-filament-deposition mechanism, we believe that there is still plenty of room for research to explore the material mechanics, printing resolutions, material versatility, and manufacturing commercialization in more industrial areas.

AUTHOR INFORMATION

Corresponding Author

Kenan Song − *Ira A. Fulton Schools of Engineering, Arizona State University, Mesa, Arizona 85212, United States;* orcid.org/0000-0002-0447-2449; Email: Kenan.song@asu.edu

Authors

Weiheng Xu − *The Polytechnic School, Ira A. Fulton Schools of Engineering, Arizona State University, Mesa, Arizona 85212, United States;* orcid.org/0000-0001-5596-4366

Yuxiang Zhu − *The Polytechnic School, Ira A. Fulton Schools of Engineering, Arizona State University, Mesa, Arizona 85212, United States;* orcid.org/0000-0001-5688-5600

Dharneedar Ravichandran − *The Polytechnic School, Ira A. Fulton Schools of Engineering, Arizona State University, Mesa, Arizona 85212, United States;* orcid.org/0000-0003-0393-7934

Sayli Jambhulkar − *The Polytechnic School, Ira A. Fulton Schools of Engineering, Arizona State University, Mesa, Arizona 85212, United States;* orcid.org/0000-0002-9171-322X

Mounika Kakarla − *Materials Science and Engineering, School for Engineering of Matter, Transport and Energy, Arizona State University, Tempe, Arizona 85281, United States*

Mohammed Bawareth − *Mechanical Engineering System, Ira A. Fulton Schools of Engineering, Arizona State University, Mesa, Arizona 85212, United States*

Shantanu Lanke − *Materials Science and Engineering, School for Engineering of Matter, Transport and Energy, Arizona State University, Tempe, Arizona 85281, United States*

Complete contact information is available at: https://pubs.acs.org/10.1021/acsanm.1c01408

Notes

The authors declare no competing financial interest.

ACKNOWLEDGMENTS

This work was funded by the U.S. National Science Foundation (EAGER 1902172).

REFERENCES

(1) Seyedin, S.; Zhang, P.; Naebe, M.; Qin, S.; Chen, J.; Wang, X.; Razal, J. M. Textile Strain Sensors: A Review of the Fabrication Technologies, Performance Evaluation and Applications. *Mater. Horiz.* **2019**, *6* (2), 219−249.

(2) Gong, Z.; Xiang, Z.; OuYang, X.; Zhang, J.; Lau, N.; Zhou, J.; Chan, C. C. Wearable Fiber Optic Technology Based on Smart Textile: A Review. *Materials* **2019**, *12*, 3311.

(3) Kamiya, R.; Cheeseman, B. A.; Popper, P.; Chou, T. W. Some Recent Advances in the Fabrication and Design of Three-Dimensional Textile Preforms: A Review. *Compos. Sci. Technol.* **2000**, *60* (1), 33−47.

(4) Heo, J. S.; Eom, J.; Kim, Y. H.; Park, S. K. Recent Progress of Textile-Based Wearable Electronics: A Comprehensive Review of Materials, Devices, and Applications. *Small* **2018**, *14*, 1703034.

(5) Song, K.; Zhang, Y.; Meng, J.; Green, E. C.; Tajaddod, N.; Li, H.; Minus, M. L. Structural Polymer-Based Carbon Nanotube Composite Fibers: Understanding the Processing-Structure-Performance Relationship. *Materials* **2013**, *6*, 2543−2577.

(6) Wu, J.; Qin, X.; Miao, C.; He, Y. B.; Liang, G.; Zhou, D.; Liu, M.; Han, C.; Li, B.; Kang, F. A Honeycomb-Cobweb Inspired Hierarchical Core-Shell Structure Design for Electrospun Silicon/Carbon Fibers as Lithium-Ion Battery Anodes. *Carbon* **2016**, *98*, 582−591.

(7) Zhang, Y.; Song, K.; Meng, J.; Minus, M. L. Tailoring Polyacrylonitrile Interfacial Morphological Structure by Crystallization in the Presence of Single-Wall Carbon Nanotubes. *ACS Appl. Mater. Interfaces* **2013**, *5* (3), 807−814.

(8) Meng, J.; Zhang, Y.; Song, K.; Minus, M. L. Forming Crystalline Polymer-Nano Interphase Structures for High-Modulus and High-Tensile/Strength Composite Fibers. *Macromol. Mater. Eng.* **2014**, *299* (2), 144−153.

(9) Song, K.; Zhang, Y.; Minus, M. L. Polymer Interphase Self-Reinforcement and Strengthening Mechanisms in Low-Loaded Nanocomposite Fibers. *Macromol. Chem. Phys.* **2015**, *216* (12), 1313−1320.

(10) Dong, K.; Peng, X.; Wang, Z. L. Fiber/Fabric-Based Piezoelectric and Triboelectric Nanogenerators for Flexible/Stretchable and Wearable Electronics and Artificial Intelligence. *Adv. Mater.* **2020**, *32* (5), 1902549.

(11) Afroj, S.; Karim, N.; Wang, Z.; Tan, S.; He, P.; Holwill, M.; Ghazaryan, D.; Fernando, A.; Novoselov, K. S. Engineering Graphene Flakes for Wearable Textile Sensors via Highly Scalable and Ultrafast Yarn Dyeing Technique. *ACS Nano* **2019**, *13* (4), 3847−3857.

(12) Song, K.; Chen, D.; Polak, R.; Rubner, M. F.; Cohen, R. E.; Askar, K. A. Enhanced Wear Resistance of Transparent Epoxy Composite Coatings with Vertically Aligned Halloysite Nanotubes. *ACS Appl. Mater. Interfaces* **2016**, *8* (51), 35552−35564.

(13) Song, K.; Polak, R.; Chen, D.; Rubner, M. F.; Cohen, R. E.; Askar, K. A. Spray-Coated Halloysite-Epoxy Composites: A Means to Create Mechanically Robust, Vertically Aligned Nanotube Composites. *ACS Appl. Mater. Interfaces* **2016**, *8* (31), 20396−20406.

(14) Maynard, A. D. Navigating the Fourth Industrial Revolution. *Nat. Nanotechnol.* **2015**, *10* (12), 1005−1006.

(15) Silva, J. V. L.; Rezende, R. A. Additive Manufacturing and Its Future Impact in Logistics. *IFAC Proc. Vol.* **2013**, *46* (24), 277−282.

(16) Ngo, T. D.; Kashani, A.; Imbalzano, G.; Nguyen, K. T. Q.; Hui, D. Additive Manufacturing (3D Printing): A Review of Materials, Methods, Applications and Challenges. *Composites, Part B* **2018**, *143*, 172−196.

(17) Power, M.; Thompson, A. J.; Anastasova, S.; Yang, G. Z. A Monolithic Force-Sensitive 3D Microgripper Fabricated on the Tip of an Optical Fiber Using 2-Photon Polymerization. *Small* **2018**, *14* (16), 1703964.

(18) Park, J. U.; Hardy, M.; Kang, S. J.; Barton, K.; Adair, K.; Mukhopadhyay, D. K.; Lee, C. Y.; Strano, M. S.; Alleyne, A. G.; Georgiadis, J. G.; Ferreira, P. M.; Rogers, J. A. High-Resolution Electrohydrodynamic Jet Printing. *Nat. Mater.* **2007**, *6* (10), 782−789.

(19) Kruth, J. P.; Wang, X.; Laoui, T.; Froyen, L. Lasers and Materials in Selective Laser Sintering. *Assem. Autom.* **2003**, *23* (4), 357−371.

(20) Xu, W.; Jambhulkar, S.; Zhu, Y.; Ravichandran, D.; Kakarla, M.; Vernon, B.; Lott, D. G.; Cornella, J. L.; Shefi, O.; Miquelard-Garnier, G.; Yang, Y.; Song, K. 3D Printing for Polymer/Particle-Based Processing: A Review. *Composites, Part B* **2021**, *223* (June), 109102.

(21) Mazzanti, V.; Malagutti, L.; Mollica, F. FDM 3D Printing of Polymers Containing Natural Fillers: A Review of Their Mechanical Properties. *Polymers (Basel, Switz.)* **2019**, *11* (7), 1094.

(22) Gurrala, P. K.; Regalla, S. P. Part Strength Evolution with Bonding between Filaments in Fused Deposition Modelling: This Paper Studies How Coalescence of Filaments Contributes to the Strength of Final FDM Part. *Virtual Phys. Prototyp.* **2014**, *9* (3), 141−149.

(23) Wickramasinghe, S.; Do, T.; Tran, P. FDM-Based 3D Printing of Polymer and Associated Composite: A Review on Mechanical Properties, Defects and Treatments. *Polymers (Basel, Switz.)* **2020**, *12*, 1529.
(24) Penumakala, P. K.; Santo, J.; Thomas, A. A Critical Review on the Fused Deposition Modeling of Thermoplastic Polymer Composites. *Composites, Part B* **2020**, *201*, 108336.
(25) Wang, X.; Jiang, M.; Zhou, Z.; Gou, J.; Hui, D. 3D Printing of Polymer Matrix Composites: A Review and Prospective. *Composites, Part B* **2017**, *110*, 442−458.
(26) Cesarano, J.; Calvert, P. Freeforming Objects with Low-Binder Slurry. U.S. Patent 6,027,326, 2000.
(27) Chen, Q.; Cao, P. F.; Advincula, R. C. Mechanically Robust, Ultraelastic Hierarchical Foam with Tunable Properties via 3D Printing. *Adv. Funct. Mater.* **2018**, *28* (21), 1800631.
(28) Naficy, S.; Jalili, R.; Aboutalebi, S. H.; Gorkin, R. A.; Konstantinov, K.; Innis, P. C.; Spinks, G. M.; Poulin, P.; Wallace, G. G. Graphene Oxide Dispersions: Tuning Rheology to Enable Fabrication. *Mater. Horiz.* **2014**, *1* (3), 326−331.
(29) Chen, Z.; Zhao, D.; Liu, B.; Nian, G.; Li, X.; Yin, J.; Qu, S.; Yang, W. 3D Printing of Multifunctional Hydrogels. *Adv. Funct. Mater.* **2019**, *29* (20), 1900971.
(30) Zhu, J.; Zhang, Q.; Yang, T.; Liu, Y.; Liu, R. 3D Printing of Multi-Scalable Structures via High Penetration near-Infrared Photopolymerization. *Nat. Commun.* **2020**, *11*, 3462.
(31) Grosskopf, A. K.; Truby, R. L.; Kim, H.; Perazzo, A.; Lewis, J. A.; Stone, H. A. Viscoplastic Matrix Materials for Embedded 3D Printing. *ACS Appl. Mater. Interfaces* **2018**, *10* (27), 23353−23361.
(32) Mu, X.; Wang, Y.; Guo, C.; Li, Y.; Ling, S.; Huang, W.; Cebe, P.; Hsu, H. H.; De Ferrari, F.; Jiang, X.; Xu, Q.; Balduini, A.; Omenetto, F. G.; Kaplan, D. L. 3D Printing of Silk Protein Structures by Aqueous Solvent-Directed Molecular Assembly. *Macromol. Biosci.* **2020**, *20* (1), 1900191.
(33) Zhang, C.; McKeon, L.; Kremer, M. P.; Park, S. H.; Ronan, O.; Seral-Ascaso, A.; Barwich, S.; Coileáin, C.; McEvoy, N.; Nerl, H. C.; Anasori, B.; Coleman, J. N.; Gogotsi, Y.; Nicolosi, V. Additive-Free MXene Inks and Direct Printing of Micro-Supercapacitors. *Nat. Commun.* **2019**, *10*, 1795.
(34) Siqueira, G.; Kokkinis, D.; Libanori, R.; Hausmann, M. K.; Gladman, A. S.; Neels, A.; Tingaut, P.; Zimmermann, T.; Lewis, J. A.; Studart, A. R. Cellulose Nanocrystal Inks for 3D Printing of Textured Cellular Architectures. *Adv. Funct. Mater.* **2017**, *27* (12), 1604619.
(35) Feilden, E.; Blanca, E. G. T.; Giuliani, F.; Saiz, E.; Vandeperre, L. Robocasting of Structural Ceramic Parts with Hydrogel Inks. *J. Eur. Ceram. Soc.* **2016**, *36* (10), 2525−2533.
(36) Li, L. Y.; Zhou, Y. M.; Gao, R. Y.; Liu, X. C.; Du, H. H.; Zhang, J. L.; Ai, X. C.; Zhang, J. P.; Fu, L. M.; Skibsted, L. H. Naturally Occurring Nanotube with Surface Modification as Biocompatible, Target-Specific Nanocarrier for Cancer Phototherapy. *Biomaterials* **2019**, *190*, 86−96.
(37) Biswas, B.; Warr, L. N.; Hilder, E. F.; Goswami, N.; Rahman, M. M.; Churchman, J. G.; Vasilev, K.; Pan, G.; Naidu, R. Biocompatible Functionalisation of Nanoclays for Improved Environmental Remediation. *Chem. Soc. Rev.* **2019**, *48* (14), 3740−3770.
(38) Revelo, C. F.; Colorado, H. A. 3D Printing of Kaolinite Clay Ceramics Using the Direct Ink Writing (DIW) Technique. *Ceram. Int.* **2018**, *44* (5), 5673−5682.
(39) Mondal, D.; Willett, T. L. Mechanical Properties of Nanocomposite Biomaterials Improved by Extrusion during Direct Ink Writing. *J. Mech. Behav. Biomed. Mater.* **2020**, *104*, 103653.
(40) Yao, B.; Chandrasekaran, S.; Zhang, H.; Ma, A.; Kang, J.; Zhang, L.; Lu, X.; Qian, F.; Zhu, C.; Duoss, E. B.; Spadaccini, C. M.; Worsley, M. A.; Li, Y. 3D-Printed Structure Boosts the Kinetics and Intrinsic Capacitance of Pseudocapacitive Graphene Aerogels. *Adv. Mater.* **2020**, *32* (8), 1906652.
(41) Lee, J. U.; Chae, S. J.; Lee, H.; Kim, G. H. A 3D Printing Strategy for Fabricating in Situ Topographical Scaffolds Using Pluronic F-127. *Addit. Manuf.* **2020**, *32*, 101023.
(42) Li, L.; Zhang, P.; Zhang, Z.; Lin, Q.; Wu, Y.; Cheng, A.; Lin, Y.; Thompson, C. M.; Smaldone, R. A.; Ke, C. Hierarchical Co-Assembly Enhanced Direct Ink Writing. *Angew. Chem.* **2018**, *130* (18), 5199−5203.
(43) Kim, F.; Kwon, B.; Eom, Y.; Lee, J. E.; Park, S.; Jo, S.; Park, S. H.; Kim, B. S.; Im, H. J.; Lee, M. H.; Min, T. S.; Kim, K. T.; Chae, H. G.; King, W. P.; Son, J. S. 3D Printing of Shape-Conformable Thermoelectric Materials Using All-Inorganic Bi2Te3-Based Inks. *Nat. Energy* **2018**, *3* (4), 301−309.
(44) Chen, K.; Kuang, X.; Li, V.; Kang, G.; Qi, H. J. Fabrication of Tough Epoxy with Shape Memory Effects by UV-Assisted Direct-Ink Write Printing. *Soft Matter* **2018**, *14* (10), 1879−1886.
(45) Lebel, L. L.; Aissa, B.; El Khakani, M. A.; Therriault, D. Ultraviolet-Assisted Direct-Write Fabrication of Carbon Nanotube/Polymer Nanocomposite Microcoils. *Adv. Mater.* **2010**, *22* (5), 592−596.
(46) Chen, Q.; Sukmanee, T.; Rong, L.; Yang, M.; Ren, J.; Ekgasit, S.; Advincula, R. A Dual Approach in Direct Ink Writing of Thermally Cured Shape Memory Rubber Toughened Epoxy. *ACS Appl. Polym. Mater.* **2020**, *2* (12), 5492−5500.
(47) Guo, Y.; Xu, J.; Yan, C.; Chen, Y.; Zhang, X.; Jia, X.; Liu, Y.; Wang, X.; Zhou, F. Direct Ink Writing of High Performance Architectured Polyimides with Low Dimensional Shrinkage. *Adv. Eng. Mater.* **2019**, *21* (5), 1801314.
(48) Wei, T. S.; Ahn, B. Y.; Grotto, J.; Lewis, J. A. 3D Printing of Customized Li-Ion Batteries with Thick Electrodes. *Adv. Mater.* **2018**, *30* (16), 1703027.
(49) Chen, H.; Wang, X.; Xue, F.; Huang, Y.; Zhou, K.; Zhang, D. 3D Printing of SiC Ceramic: Direct Ink Writing with a Solution of Preceramic Polymers. *J. Eur. Ceram. Soc.* **2018**, *38* (16), 5294−5300.
(50) Hasib, A. G.; Niauzorau, S.; Xu, W.; Niverty, S.; Kublik, N.; Williams, J.; Chawla, N.; Song, K.; Azeredo, B. Rheology Scaling of Spherical Metal Powders Dispersed in Thermoplastics and Its Correlation to the Extrudability of Filaments for 3D Printing. *Addit. Manuf.* **2021**, *41*, 101967.
(51) Zhang, B.; Chung, S. H.; Barker, S.; Craig, D.; Narayan, R. J.; Huang, J. Direct Ink Writing of Polycaprolactone/Polyethylene Oxide Based 3D Constructs. *Prog. Nat. Sci.* **2021**, *31* (2), 180−191.
(52) Jin, Y.; Compaan, A.; Bhattacharjee, T.; Huang, Y. Granular Gel Support-Enabled Extrusion of Three-Dimensional Alginate and Cellular Structures. *Biofabrication* **2016**, *8*, 025016.
(53) Jin, Y.; Compaan, A.; Chai, W.; Huang, Y. Functional Nanoclay Suspension for Printing-Then-Solidification of Liquid Materials. *ACS Appl. Mater. Interfaces* **2017**, *9* (23), 20057−20066.
(54) O'Bryan, C. S.; Kabb, C. P.; Sumerlin, B. S.; Angelini, T. E. Jammed Polyelectrolyte Microgels for 3D Cell Culture Applications: Rheological Behavior with Added Salts. *ACS Appl. Bio Mater.* **2019**, *2* (4), 1509−1517.
(55) Li, V. C. F.; Kuang, X.; Hamel, C. M.; Roach, D.; Deng, Y.; Qi, H. J. Cellulose Nanocrystals Support Material for 3D Printing Complexly Shaped Structures via Multi-Materials-Multi-Methods Printing. *Addit. Manuf.* **2019**, *28*, 14−22.
(56) Bhattacharjee, T.; Zehnder, S. M.; Rowe, K. G.; Jain, S.; Nixon, R. M.; Sawyer, W. G.; Angelini, T. E. Writing in the Granular Gel Medium. *Sci. Adv.* **2015**, *1* (8), No. e1500655.
(57) Friedrich, L.; Begley, M. Changes in Filament Microstructures During Direct Ink Writing with a Yield Stress Fluid Support. *ACS Appl. Polym. Mater.* **2020**, *2* (7), 2528−2540.
(58) Hausmann, M. K.; Siqueira, G.; Libanori, R.; Kokkinis, D.; Neels, A.; Zimmermann, T.; Studart, A. R. Complex-Shaped Cellulose Composites Made by Wet Densification of 3D Printed Scaffolds. *Adv. Funct. Mater.* **2020**, *30* (4), 1904127.
(59) Leppiniemi, J.; Lahtinen, P.; Paajanen, A.; Mahlberg, R.; Metsä-Kortelainen, S.; Pinomaa, T.; Pajari, H.; Vikholm-Lundin, I.; Pursula, P.; Hytönen, V. P. 3D-Printable Bioactivated Nanocellulose-Alginate Hydrogels. *ACS Appl. Mater. Interfaces* **2017**, *9* (26), 21959−21970.
(60) Li, Y.; Zhu, H.; Wang, Y.; Ray, U.; Zhu, S.; Dai, J.; Chen, C.; Fu, K.; Jang, S.-H.; Henderson, D.; Li, T.; Hu, L. Cellulose-Nanofiber-

https://doi.org/10.1021/acsanm.1c01408
ACS Appl. Nano Mater. 2021, 4, 7538−7562

Enabled 3D Printing of a Carbon-Nanotube Microfiber Network. *Small Methods* **2017**, *1* (10), 1700222.
(61) Saeidijavash, M.; Garg, J.; Grady, B.; Smith, B.; Li, Z.; Young, R. J.; Tarannum, F.; Bel Bekri, N. High Thermal Conductivity through Simultaneously Aligned Polyethylene Lamellae and Graphene Nanoplatelets. *Nanoscale* **2017**, *9* (35), 12867−12873.
(62) Wang, W.; Murthy, N. S.; Chae, H. G.; Kumar, S. Structural Changes during Deformation in Carbon Nanotube-Reinforced Polyacrylonitrile Fibers. *Polymer* **2008**, *49* (8), 2133−2145.
(63) Xu, W.; Jambhulkar, S.; Verma, R.; Franklin, R.; Ravichandran, D.; Song, K. In Situ Alignment of Graphene Nanoplatelets in Poly(Vinyl Alcohol) Nanocomposite Fibers with Controlled Stepwise Interfacial Exfoliation. *Nanoscale Adv.* **2019**, *1* (7), 2510−2517.
(64) Tajaddod, N.; Song, K.; Green, E. C.; Zhang, Y.; Minus, M. L. Exfoliation of Boron Nitride Platelets by Enhanced Interfacial Interaction with Polyethylene. *Macromol. Mater. Eng.* **2016**, *301* (3), 315−327.
(65) Xu, Y.; Hong, W.; Bai, H.; Li, C.; Shi, G. Strong and Ductile Poly(Vinyl Alcohol)/Graphene Oxide Composite Films with a Layered Structure. *Carbon* **2009**, *47* (15), 3538−3543.
(66) Li, Z.; Young, R. J.; Wilson, N. R.; Kinloch, I. A.; Vallés, C.; Li, Z. Effect of the Orientation of Graphene-Based Nanoplatelets upon the Young's Modulus of Nanocomposites. *Compos. Sci. Technol.* **2016**, *123*, 125−133.
(67) Liu, G. R. A Step-by-Step Method of Rule-of-Mixture of Fiber- and Particle-Reinforced Composite Materials. *Compos. Struct.* **1997**, *40* (3−4), 313−322.
(68) Souier, T.; Santos, S.; Al Ghaferi, A.; Stefancich, M.; Chiesa, M. Enhanced Electrical Properties of Vertically Aligned Carbon Nanotube-Epoxy Nanocomposites with High Packing Density. *Nanoscale Res. Lett.* **2012**, *7*, 630.
(69) Zhang, S.; Koziol, K. K. K.; Kinloch, I. A.; Windle, A. H. Macroscopic Fibers of Well-Aligned Carbon Nanotubes by Wet Spinning. *Small* **2008**, *4* (8), 1217−1222.
(70) Wan, F.; Ping, H.; Wang, W.; Zou, Z.; Xie, H.; Su, B.; Liu, D.; Fu, Z. Hydroxyapatite-Reinforced Alginate Fibers with Bioinspired Dually Aligned Architectures. *Carbohydr. Polym.* **2021**, *267*, 118167.
(71) Feilden, E.; Ferraro, C.; Zhang, Q.; García-Tuñón, E.; D'Elia, E.; Giuliani, F.; Vandeperre, L.; Saiz, E. 3D Printing Bioinspired Ceramic Composites. *Sci. Rep.* **2017**, *7*, 13759.
(72) Hausmann, M. K.; Rühs, P. A.; Siqueira, G.; Läuger, J.; Libanori, R.; Zimmermann, T.; Studart, A. R. Dynamics of Cellulose Nanocrystal Alignment during 3D Printing. *ACS Nano* **2018**, *12*, 6926−6937.
(73) Kularatne, R. S.; Kim, H.; Boothby, J. M.; Ware, T. H. Liquid Crystal Elastomer Actuators: Synthesis, Alignment, and Applications. *J. Polym. Sci., Part B: Polym. Phys.* **2017**, *55* (5), 395−411.
(74) White, T. J.; Broer, D. J. Programmable and Adaptive Mechanics with Liquid Crystal Polymer Networks and Elastomers. *Nat. Mater.* **2015**, *14* (11), 1087−1098.
(75) Pozo, M.; Liu, L.; Pilz da Cunha, M.; Broer, D. J.; Schenning, A. P. H. J. Direct Ink Writing of a Light-Responsive Underwater Liquid Crystal Actuator with Atypical Temperature-Dependent Shape Changes. *Adv. Funct. Mater.* **2020**, *30* (50), 2005560.
(76) Li, T.; Chen, C.; Brozena, A. H.; Zhu, J. Y.; Xu, L.; Driemeier, C.; Dai, J.; Rojas, O. J.; Isogai, A.; Wågberg, L.; Hu, L. Developing Fibrillated Cellulose as a Sustainable Technological Material. *Nature* **2021**, *590* (7844), 47−56.
(77) Ajdary, R.; Tardy, B. L.; Mattos, B. D.; Bai, L.; Rojas, O. J. Plant Nanomaterials and Inspiration from Nature: Water Interactions and Hierarchically Structured Hydrogels. *Adv. Mater.* **2021**, *33* (28), 2001085.
(78) Foster, E. J.; Moon, R. J.; Agarwal, U. P.; Bortner, M. J.; Bras, J.; Camarero-Espinosa, S.; Chan, K. J.; Clift, M. J. D.; Cranston, E. D.; Eichhorn, S. J.; Fox, D. M.; Hamad, W. Y.; Heux, L.; Jean, B.; Korey, M.; Nieh, W.; Ong, K. J.; Reid, M. S.; Renneckar, S.; Roberts, R.; Shatkin, J. A.; Simonsen, J.; Stinson-Bagby, K.; Wanasekara, N.; Youngblood, J. Current Characterization Methods for Cellulose Nanomaterials. *Chem. Soc. Rev.* **2018**, *47* (8), 2609−2679.
(79) Kargarzadeh, H.; Mariano, M.; Gopakumar, D.; Ahmad, I.; Thomas, S.; Dufresne, A.; Huang, J.; Lin, N. Advances in Cellulose Nanomaterials. *Cellulose* **2018**, *25* (4), 2151−2189.
(80) Liu, J.; Li, W.; Guo, Y.; Zhang, H.; Zhang, Z. Improved Thermal Conductivity of Thermoplastic Polyurethane via Aligned Boron Nitride Platelets Assisted by 3D Printing. *Composites, Part A* **2019**, *120*, 140−146.
(81) Jakus, A. E.; Secor, E. B.; Rutz, A. L.; Jordan, S. W.; Hersam, M. C.; Shah, R. N. Three-Dimensional Printing of High-Content Graphene Scaffolds for Electronic and Biomedical Applications. *ACS Nano* **2015**, *9* (4), 4636−4648.
(82) Zhang, C. J.; Anasori, B.; Seral-Ascaso, A.; Park, S. H.; McEvoy, N.; Shmeliov, A.; Duesberg, G. S.; Coleman, J. N.; Gogotsi, Y.; Nicolosi, V. Transparent, Flexible, and Conductive 2D Titanium Carbide (MXene) Films with High Volumetric Capacitance. *Adv. Mater.* **2017**, *29* (36), 1702678.
(83) Qian, Y.; Li, C.; Qi, Y.; Zhong, J. 3D Printing of Graphene Oxide Composites with Well Controlled Alignment. *Carbon* **2021**, *171*, 777−784.
(84) Cheng, M.; Ramasubramanian, A.; Rasul, M. G.; Jiang, Y.; Yuan, Y.; Foroozan, T.; Deivanayagam, R.; Tamadoni Saray, M.; Rojaee, R.; Song, B.; Yurkiv, V. R.; Pan, Y.; Mashayek, F.; Shahbazian-Yassar, R. Direct Ink Writing of Polymer Composite Electrolytes with Enhanced Thermal Conductivities. *Adv. Funct. Mater.* **2021**, *31* (4), 2006683.
(85) Zhu, Y.; Xie, J.; Pei, A.; Liu, B.; Wu, Y.; Lin, D.; Li, J.; Wang, H.; Chen, H.; Xu, J.; Yang, A.; Wu, C. L.; Wang, H.; Chen, W.; Cui, Y. Fast Lithium Growth and Short Circuit Induced by Localized-Temperature Hotspots in Lithium Batteries. *Nat. Commun.* **2019**, *10*, 2067.
(86) Gu, X.; Shaw, L.; Gu, K.; Toney, M. F.; Bao, Z. The Meniscus-Guided Deposition of Semiconducting Polymers. *Nat. Commun.* **2018**, *9*, 534.
(87) Gu, X.; Zhou, Y.; Gu, K.; Kurosawa, T.; Guo, Y.; Li, Y.; Lin, H.; Schroeder, B. C.; Yan, H.; Molina-Lopez, F.; Tassone, C. J.; Wang, C.; Mannsfeld, S. C. B.; Yan, H.; Zhao, D.; Toney, M. F.; Bao, Z. Roll-to-Roll Printed Large-Area All-Polymer Solar Cells with 5% Efficiency Based on a Low Crystallinity Conjugated Polymer Blend. *Adv. Energy Mater.* **2017**, *7*, 1602742.
(88) Jambhulkar, S.; Xu, W.; Ravichandran, D.; Prakash, J.; Mada Kannan, A. N.; Song, K. Scalable Alignment and Selective Deposition of Nanoparticles for Multifunctional Sensor Applications. *Nano Lett.* **2020**, *20* (5), 3199−3206.
(89) Jambhulkar, S.; Liu, S.; Vala, P.; Xu, W.; Ravichandran, D.; Zhu, Y.; Bi, K.; Nian, Q.; Chen, X.; Song, K. Aligned Ti 3C2 Tx MXene for 3D Micropatterning via Additive Manufacturing. *ACS Nano* **2021**, *15*, 12057.
(90) Diao, Y.; Shaw, L.; Bao, Z.; Mannsfeld, S. C. B. Morphology Control Strategies for Solution-Processed Organic Semiconductor Thin Films. *Energy Environ. Sci.* **2014**, *7* (7), 2145−2159.
(91) Hu, J.; Yu, M. F. Meniscus-Confined Three-Dimensional Electrodeposition for Direct Writing of Wire Bonds. *Science (Washington, DC, U. S.)* **2010**, *329* (5989), 313−316.
(92) Kim, J. T.; Seol, S. K.; Pyo, J.; Lee, J. S.; Je, J. H.; Margaritondo, G. Three-Dimensional Writing of Conducting Polymer Nanowire Arrays by Meniscus-Guided Polymerization. *Adv. Mater.* **2011**, *23* (17), 1968−1970.
(93) Yang, J.; Chen, M.; Lee, H.; Xu, Z.; Zhou, Z.; Feng, S. P.; Kim, J. T. Three-Dimensional Printing of Self-Assembled Dipeptides. *ACS Appl. Mater. Interfaces* **2021**, *13* (17), 20573−20580.
(94) Chen, M.; Yang, J.; Wang, Z.; Xu, Z.; Lee, H.; Lee, H.; Zhou, Z.; Feng, S. P.; Lee, S.; Pyo, J.; Seol, S. K.; Ki, D. K.; Kim, J. T. 3D Nanoprinting of Perovskites. *Adv. Mater.* **2019**, *31*, 1904073.
(95) Oener, S. Z.; Khoram, P.; Brittman, S.; Mann, S. A.; Zhang, Q.; Fan, Z.; Boettcher, S. W.; Garnett, E. C. Perovskite Nanowire Extrusion. *Nano Lett.* **2017**, *17* (11), 6557−6563.
(96) Kim, J. H.; Chang, W. S.; Kim, D.; Yang, J. R.; Han, J. T.; Lee, G. W.; Kim, J. T.; Seol, S. K. 3D Printing of Reduced Graphene Oxide Nanowires. *Adv. Mater.* **2015**, *27* (1), 157−161.

https://doi.org/10.1021/acsanm.1c01408
ACS Appl. Nano Mater. 2021, 4, 7538−7562

(97) Kim, J. H.; Lee, S.; Wajahat, M.; Jeong, H.; Chang, W. S.; Jeong, H. J.; Yang, J. R.; Kim, J. T.; Seol, S. K. Three-Dimensional Printing of Highly Conductive Carbon Nanotube Microarchitectures with Fluid Ink. *ACS Nano* **2016**, *10* (9), 8879−8887.
(98) Wajahat, M.; Lee, S.; Kim, J. H.; Chang, W. S.; Pyo, J.; Cho, S. H.; Seol, S. K. Flexible Strain Sensors Fabricated by Meniscus-Guided Printing of Carbon Nanotube-Polymer Composites. *ACS Appl. Mater. Interfaces* **2018**, *10* (23), 19999−20005.
(99) Deville, S.; Saiz, E.; Nalla, R. K.; Tomsia, A. P. Freezing as a Path to Build Complex Composites. *Science (Washington, DC, U. S.)* **2006**, *311* (5760), 515−518.
(100) Du, G.; Mao, A.; Yu, J.; Hou, J.; Zhao, N.; Han, J.; Zhao, Q.; Gao, W.; Xie, T.; Bai, H. Nacre-Mimetic Composite with Intrinsic Self-Healing and Shape-Programming Capability. *Nat. Commun.* **2019**, *10*, 800.
(101) Wang, X.; Zhai, H.; Qie, B.; Cheng, Q.; Li, A.; Borovilas, J.; Xu, B.; Shi, C.; Jin, T.; Liao, X.; Li, Y.; He, X.; Du, S.; Fu, Y.; Dontigny, M.; Zaghib, K.; Yang, Y. Rechargeable Solid-State Lithium Metal Batteries with Vertically Aligned Ceramic Nanoparticle/Polymer Composite Electrolyte. *Nano Energy* **2019**, *60* (March), 205−212.
(102) Bai, H.; Chen, Y.; Delattre, B.; Tomsia, A. P.; Ritchie, R. O. Bioinspired Large-Scale Aligned Porous Materials Assembled with Dual Temperature Gradients. *Sci. Adv.* **2015**, *1*, No. e1500849.
(103) Bai, H.; Walsh, F.; Gludovatz, B.; Delattre, B.; Huang, C.; Chen, Y.; Tomsia, A. P.; Ritchie, R. O. Bioinspired Hydroxyapatite/Poly(Methyl Methacrylate) Composite with a Nacre-Mimetic Architecture by a Bidirectional Freezing Method. *Adv. Mater.* **2016**, *28* (1), 50−56.
(104) Zhai, H.; Xu, P.; Ning, M.; Cheng, Q.; Mandal, J.; Yang, Y. A Flexible Solid Composite Electrolyte with Vertically Aligned and Connected Ion-Conducting Nanoparticles for Lithium Batteries. *Nano Lett.* **2017**, *17* (5), 3182−3187.
(105) Pang, Y.; Yang, J.; Curtis, T. E.; Luo, S.; Huang, D.; Feng, Z.; Morales-Ferreiro, J. O.; Sapkota, P.; Lei, F.; Zhang, J.; Zhang, Q.; Lee, E.; Huang, Y.; Guo, R.; Ptasinska, S.; Roeder, R. K.; Luo, T. Exfoliated Graphene Leads to Exceptional Mechanical Properties of Polymer Composite Films. *ACS Nano* **2019**, *13* (2), 1097−1106.
(106) Cui, Y.; Gong, H.; Wang, Y.; Li, D.; Bai, H. A Thermally Insulating Textile Inspired by Polar Bear Hair. *Adv. Mater.* **2018**, *30*, 1706807.
(107) Li, W.; Li, Y.; Su, M.; An, B.; Liu, J.; Su, D.; Li, L.; Li, F.; Song, Y. Printing Assembly and Structural Regulation of Graphene towards Three-Dimensional Flexible Micro-Supercapacitors. *J. Mater. Chem. A* **2017**, *5* (31), 16281−16288.
(108) Wei, X.; Liu, C.; Wang, Z.; Luo, Y. 3D Printed Core-Shell Hydrogel Fiber Scaffolds with NIR-Triggered Drug Release for Localized Therapy of Breast Cancer. *Int. J. Pharm.* **2020**, *580*, 119219.
(109) Zhu, K.; Shin, S. R.; van Kempen, T.; Li, Y. C.; Ponraj, V.; Nasajpour, A.; Mandla, S.; Hu, N.; Liu, X.; Leijten, J.; Lin, Y. D.; Hussain, M. A.; Zhang, Y. S.; Tamayol, A.; Khademhosseini, A. Gold Nanocomposite Bioink for Printing 3D Cardiac Constructs. *Adv. Funct. Mater.* **2017**, *27* (12), 1605352.
(110) Cui, Q.; Bell, D. J.; Rauer, S. B.; Wessling, M. Wet-Spinning of Biocompatible Core-Shell Polyelectrolyte Complex Fibers for Tissue Engineering. *Adv. Mater. Interfaces* **2020**, *7* (23), 2000849.
(111) Chen, C.; Chen, X.; Zhang, H.; Zhang, Q.; Wang, L.; Li, C.; Dai, B.; Yang, J.; Liu, J.; Sun, D. Electrically-Responsive Core-Shell Hybrid Microfibers for Controlled Drug Release and Cell Culture. *Acta Biomater.* **2017**, *55*, 434−442.
(112) Ding, Y.; Dou, C.; Chang, S.; Xie, Z.; Yu, D. G.; Liu, Y.; Shao, J. Core-Shell Eudragit S100 Nanofibers Preparedvia Triaxial Electrospinning to Providea Colon-Targeted Extended Drug Release. *Polymers (Basel, Switz.)* **2020**, *12* (9), 2034.
(113) Lu, L.; Yang, B.; Zhai, Y.; Liu, J. Electrospinning Core-Sheath Piezoelectric Microfibers for Self-Powered Stitchable Sensor. *Nano Energy* **2020**, *76*, 104966.
(114) Park, J. J.; Hyun, W. J.; Mun, S. C.; Park, Y. T.; Park, O. O. Highly Stretchable and Wearable Graphene Strain Sensors with Controllable Sensitivity for Human Motion Monitoring. *ACS Appl. Mater. Interfaces* **2015**, *7* (11), 6317−6324.
(115) Liang, H.; Lin, J.; Jia, H.; Chen, S.; Qi, J.; Cao, J.; Lin, T.; Fei, W.; Feng, J. Hierarchical NiCo-LDH@NiOOH Core-Shell Heterostructure on Carbon Fiber Cloth as Battery-like Electrode for Supercapacitor. *J. Power Sources* **2018**, *378*, 248−254.
(116) Hwang, T. H.; Lee, Y. M.; Kong, B. S.; Seo, J. S.; Choi, J. W. Electrospun Core-Shell Fibers for Robust Silicon Nanoparticle-Based Lithium Ion Battery Anodes. *Nano Lett.* **2012**, *12* (2), 802−807.
(117) Zhou, X.; Xu, X.; Zuo, Y.; Liao, M.; Shi, X.; Chen, C.; Xie, S.; Zhou, P.; Sun, X.; Peng, H. A Fiber-Shaped Light-Emitting Pressure Sensor for Visualized Dynamic Monitoring. *J. Mater. Chem. C* **2020**, *8* (3), 935−942.
(118) Liu, D.; Ren, J.; Wang, J.; Xing, W.; Qian, Q.; Chen, H.; Zhou, N. Customizable and Stretchable Fibre-Shaped Electroluminescent Devices: Via Mulitcore-Shell Direct Ink Writing. *J. Mater. Chem. C* **2020**, *8* (43), 15092−15098.
(119) Le, V. T.; Kim, H.; Ghosh, A.; Kim, J.; Chang, J.; Vu, Q. A.; Pham, D. T.; Lee, J. H.; Kim, S. W.; Lee, Y. H. Coaxial Fiber Supercapacitor Using All-Carbon Material Electrodes. *ACS Nano* **2013**, *7* (7), 5940−5947.
(120) Yu, X.; Fu, Y.; Cai, X.; Kafafy, H.; Wu, H.; Peng, M.; Hou, S.; Lv, Z.; Ye, S.; Zou, D. Flexible Fiber-Type Zinc-Carbon Battery Based on Carbon Fiber Electrodes. *Nano Energy* **2013**, *2* (6), 1242−1248.
(121) Zhao, J.; Lu, H.; Zhang, Y.; Yu, S.; Malyi, O. I.; Zhao, X.; Wang, L.; Wang, H.; Peng, J.; Li, X.; Zhang, Y.; Chen, S.; Pan, H.; Xing, G.; Lu, C.; Tang, Y.; Chen, X. Direct Coherent Multi-Ink Printing of Fabric Supercapacitors. *Sci. Adv.* **2021**, *7* (3), No. eabd6978.
(122) Khudiyev, T.; Lee, J. T.; Cox, J. R.; Argentieri, E.; Loke, G.; Yuan, R.; Noel, G. H.; Tatara, R.; Yu, Y.; Logan, F.; Joannopoulos, J.; Shao-Horn, Y.; Fink, Y. 100 m Long Thermally Drawn Supercapacitor Fibers with Applications to 3D Printing and Textiles. *Adv. Mater.* **2020**, *32* (49), 2004971.
(123) Skylar-Scott, M. A.; Mueller, J.; Visser, C. W.; Lewis, J. A. Voxelated Soft Matter via Multimaterial Multinozzle 3D Printing. *Nature* **2019**, *575* (7782), 330−335.
(124) Chen, J.; Wen, H.; Zhang, G.; Lei, F.; Feng, Q.; Liu, Y.; Cao, X.; Dong, H. Multifunctional Conductive Hydrogel/Thermochromic Elastomer Hybrid Fibers with a Core-Shell Segmental Configuration for Wearable Strain and Temperature Sensors. *ACS Appl. Mater. Interfaces* **2020**, *12* (6), 7565−7574.
(125) Chen, Y.; Liu, Y.; Ren, J.; Yang, W.; Shang, E.; Ma, K.; Zhang, L.; Jiang, J.; Sun, X. Conformable Core-Shell Fiber Tactile Sensor by Continuous Tubular Deposition Modeling with Water-Based Sacrificial Coaxial Writing. *Mater. Des.* **2020**, *190*, 108567.
(126) Chen, Y.; Deng, Z.; Ouyang, R.; Zheng, R.; Jiang, Z.; Bai, H.; Xue, H. 3D Printed Stretchable Smart Fibers and Textiles for Self-Powered e-Skin. *Nano Energy* **2021**, *84*, 105866.
(127) Athanasiadis, M.; Pak, A.; Afanasenkau, D.; Minev, I. R. Direct Writing of Elastic Fibers with Optical, Electrical, and Microfluidic Functionality. *Adv. Mater. Technol.* **2019**, *4* (7), 1800659.
(128) Zhang, M.; Zhao, M.; Jian, M.; Wang, C.; Yu, A.; Yin, Z.; Liang, X.; Wang, H.; Xia, K.; Liang, X.; Zhai, J.; Zhang, Y. Printable Smart Pattern for Multifunctional Energy-Management E-Textile. *Matter* **2019**, *1* (1), 168−179.
(129) Gao, G.; Park, J. Y.; Kim, B. S.; Jang, J.; Cho, D. W. Coaxial Cell Printing of Freestanding, Perfusable, and Functional In Vitro Vascular Models for Recapitulation of Native Vascular Endothelium Pathophysiology. *Adv. Healthcare Mater.* **2018**, *7*, 1801102.
(130) Colosi, C.; Shin, S. R.; Manoharan, V.; Massa, S.; Costantini, M.; Barbetta, A.; Dokmeci, M. R.; Dentini, M.; Khademhosseini, A. Microfluidic Bioprinting of Heterogeneous 3D Tissue Constructs Using Low-Viscosity Bioink. *Adv. Mater.* **2016**, *28* (4), 677−684a.
(131) Wang, Z.; Ren, J.; Liu, R.; Sun, X.; Huang, D.; Xu, W.; Jiang, J.; Ma, K.; Liu, Y. Three Dimensional Core-Shell Structured Liquid Metal/Elastomer Composite via Coaxial Direct Ink Writing for Electromagnetic Interference Shielding. *Composites, Part A* **2020**, *136*, 105957.

https://doi.org/10.1021/acsanm.1c01408
ACS Appl. Nano Mater. 2021, 4, 7538−7562

(132) Xu, J.; Zhang, X.; Liu, Y.; Zhang, Y.; Nie, H. Y.; Zhang, G.; Gao, W. Selective Coaxial Ink 3D Printing for Single-Pass Fabrication of Smart Elastomeric Foam with Embedded Stretchable Sensor. *Addit. Manuf.* **2020**, *36*, 101487.
(133) Moon, Y. W.; Choi, I. J.; Koh, Y. H.; Kim, H. E. Macroporous Alumina Scaffolds Consisting of Highly Microporous Hollow Filaments Using Three-Dimensional Ceramic/Camphene-Based Co-Extrusion. *J. Eur. Ceram. Soc.* **2015**, *35* (16), 4623−4627.
(134) Paredes, C.; Martínez-Vázquez, F. J.; Pajares, A.; Miranda, P. Novel Strategy for Toughening Robocast Bioceramic Scaffolds Using Polymeric Cores. *Ceram. Int.* **2019**, *45* (15), 19572−19576.
(135) Chortos, A.; Mao, J.; Mueller, J.; Hajiesmaili, E.; Lewis, J. A.; Clarke, D. R. Printing Reconfigurable Bundles of Dielectric Elastomer Fibers. *Adv. Funct. Mater.* **2021**, *31*, 2010643.
(136) Xia, Y.; Lu, Z.; Cao, J.; Miao, K.; Li, J.; Li, D. Microstructure and Mechanical Property of Cf/SiC Core/Shell Composite Fabricated by Direct Ink Writing. *Scr. Mater.* **2019**, *165*, 84−88.
(137) Chen, S.; Huang, T.; Zuo, H.; Qian, S.; Guo, Y.; Sun, L.; Lei, D.; Wu, Q.; Zhu, B.; He, C.; Mo, X.; Jeffries, E.; Yu, H.; You, Z. A Single Integrated 3D-Printing Process Customizes Elastic and Sustainable Triboelectric Nanogenerators for Wearable Electronics. *Adv. Funct. Mater.* **2018**, *28* (46), 1805108.
(138) Chávez-Madero, C.; De León-Derby, M. D.; Samandari, M.; Ceballos-González, C. F.; Bolívar-Monsalve, E. J.; Mendoza-Buenrostro, C.; Holmberg, S.; Garza-Flores, N. A.; Almajhadi, M. A.; González-Gamboa, I.; Yee-De León, J. F.; Martínez-Chapa, S. O.; Rodríguez, C. A.; Wickramasinghe, H. K.; Madou, M.; Dean, D.; Khademhosseini, A.; Zhang, Y. S.; Alvarez, M. M.; Trujillo-De Santiago, G. Using Chaotic Advection for Facile High-Throughput Fabrication of Ordered Multilayer Micro-and Nanostructures: Continuous Chaotic Printing. *Biofabrication* **2020**, *12* (3), 035023.
(139) Liu, W.; Zhang, Y. S.; Heinrich, M. A.; De Ferrari, F.; Jang, H. L.; Bakht, S. M.; Alvarez, M. M.; Yang, J.; Li, Y. C.; Trujillo-de Santiago, G.; Miri, A. K.; Zhu, K.; Khoshakhlagh, P.; Prakash, G.; Cheng, H.; Guan, X.; Zhong, Z.; Ju, J.; Zhu, G. H.; Jin, X.; Shin, S. R.; Dokmeci, M. R.; Khademhosseini, A. Rapid Continuous Multimaterial Extrusion Bioprinting. *Adv. Mater.* **2017**, *29* (3), 1604630.
(140) Bolívar-Monsalve, E. J.; Ceballos-González, C. F.; Borrayo-Montaño, K. I.; Quevedo-Moreno, D. A.; Yee-de León, J. F.; Khademhosseini, A.; Weiss, P. S.; Alvarez, M. M.; Trujillo-de Santiago, G. Continuous Chaotic Bioprinting of Skeletal Muscle-like Constructs. *Bioprinting* **2021**, *21*, No. e00125.
(141) Zhou, X.; Parida, K.; Halevi, O.; Liu, Y.; Xiong, J.; Magdassi, S.; Lee, P. S. All 3D-Printed Stretchable Piezoelectric Nanogenerator with Non-Protruding Kirigami Structure. *Nano Energy* **2020**, *72*, 104676.
(142) Jiang, Z.; Erol, O.; Chatterjee, D.; Xu, W.; Hibino, N.; Romer, L. H.; Kang, S. H.; Gracias, D. H. Direct Ink Writing of Poly(Tetrafluoroethylene) (PTFE) with Tunable Mechanical Properties. *ACS Appl. Mater. Interfaces* **2019**, *11* (31), 28289−28295.
(143) Sajadi, S. M.; Boul, P. J.; Thaemlitz, C.; Meiyazhagan, A. K.; Puthirath, A. B.; Tiwary, C. S.; Rahman, M. M.; Ajayan, P. M. Direct Ink Writing of Cement Structures Modified with Nanoscale Additive. *Adv. Eng. Mater.* **2019**, *21* (8), 1801380.
(144) Wang, Y.; Zhang, Y.; Wang, G.; Shi, X.; Qiao, Y.; Liu, J.; Liu, H.; Ganesh, A.; Li, L. Direct Graphene-Carbon Nanotube Composite Ink Writing All-Solid-State Flexible Microsupercapacitors with High Areal Energy Density. *Adv. Funct. Mater.* **2020**, *30* (16), 1907284.
(145) Orangi, J.; Hamade, F.; Davis, V. A.; Beidaghi, M. 3D Printing of Additive-Free 2D Ti3C2Tx (MXene) Ink for Fabrication of Micro-Supercapacitors with Ultra-High Energy Densities. *ACS Nano* **2020**, *14* (1), 640−650.
(146) Cheng, Q.; Liu, Y.; Lyu, J.; Lu, Q.; Zhang, X.; Song, W. 3D Printing-Directed Auxetic Kevlar Aerogel Architectures with Multiple Functionalization Options. *J. Mater. Chem. A* **2020**, *8*, 14243−14253.
(147) Imtiaz, B.; Shepelin, N. A.; Sherrell, P. C.; Kentish, S. E.; Ellis, A. V. Direct Ink Writing of Dehydrofluorinated Poly (Vinylidene Difluoride) for Microfiltration Membrane Fabrication. *J. Membr. Sci.* **2021**, *632*, 119347.
(148) Koh, J. J.; Lim, G. J. H.; Zhou, X.; Zhang, X.; Ding, J.; He, C. 3D-Printed Anti-Fouling Cellulose Mesh for Highly Efficient Oil/Water Separation Applications. *ACS Appl. Mater. Interfaces* **2019**, *11* (14), 13787−13795.
(149) Yuan, J.; Yi, C.; Jiang, H.; Liu, F.; Cheng, G. J. Direct Ink Writing of Hierarchically Porous Cellulose/Alginate Monolithic Hydrogel as a Highly Effective Adsorbent for Environmental Applications. *ACS Appl. Polym. Mater.* **2021**, *3* (2), 699−709.
(150) Sajadi, S. M.; Enayat, S.; Vásárhelyi, L.; Alabastri, A.; Lou, M.; Sassi, L. M.; Kutana, A.; Bhowmick, S.; Durante, C.; Kukovecz, Á.; Puthirath, A. B.; Kónya, Z.; Vajtai, R.; Boul, P.; Tiwary, C. S.; Rahman, M. M.; Ajayan, P. M. Three-Dimensional Printing of Complex Graphite Structures. *Carbon* **2021**, *181*, 260−269.
(151) Cheng, Y.; Chan, K. H.; Wang, X. Q.; Ding, T.; Li, T.; Lu, X.; Ho, G. W. Direct-Ink-Write 3D Printing of Hydrogels into Biomimetic Soft Robots. *ACS Nano* **2019**, *13* (11), 13176−13184.
(152) Chen, Y.; Han, P.; Vandi, L. J.; Dehghan-Manshadi, A.; Humphry, J.; Kent, D.; Stefani, I.; Lee, P.; Heitzmann, M.; Cooper-White, J.; Dargusch, M. A Biocompatible Thermoset Polymer Binder for Direct Ink Writing of Porous Titanium Scaffolds for Bone Tissue Engineering. *Mater. Sci. Eng., C* **2019**, *95*, 160−165.
(153) Fu, Q.; Saiz, E.; Tomsia, A. P. Direct Ink Writing of Highly Porous and Strong Glass Scaffolds for Load-Bearing Bone Defects Repair and Regeneration. *Acta Biomater.* **2011**, *7* (10), 3547−3554.
(154) Kuo, C. Y.; Eranki, A.; Placone, J. K.; Rhodes, K. R.; Aranda-Espinoza, H.; Fernandes, R.; Fisher, J. P.; Kim, P. C. W. Development of a 3D Printed, Bioengineered Placenta Model to Evaluate the Role of Trophoblast Migration in Preeclampsia. *ACS Biomater. Sci. Eng.* **2016**, *2* (10), 1817−1826.
(155) Collino, R. R.; Ray, T. R.; Fleming, R. C.; Cornell, J. D.; Compton, B. G.; Begley, M. R. Deposition of Ordered Two-Phase Materials Using Microfluidic Print Nozzles with Acoustic Focusing. *Extrem. Mech. Lett.* **2016**, *8*, 96−106.
(156) Goh, G. L.; Agarwala, S.; Yeong, W. Y. Directed and On-Demand Alignment of Carbon Nanotube: A Review toward 3D Printing of Electronics. *Adv. Mater. Interfaces* **2019**, *6* (4), 1801318.
(157) Yang, Y.; Li, X.; Chu, M.; Sun, H.; Jin, J.; Yu, K.; Wang, Q.; Zhou, Q.; Chen, Y. Electrically Assisted 3D Printing of Nacre-Inspired Structures with Self-Sensing Capability. *Sci. Adv.* **2019**, *5* (4), No. eaau9490.
(158) Sazan, H.; Piperno, S.; Layani, M.; Magdassi, S.; Shpaisman, H. Directed Assembly of Nanoparticles into Continuous Microstructures by Standing Surface Acoustic Waves. *J. Colloid Interface Sci.* **2019**, *536*, 701−709.
(159) Li, X.; Shan, W.; Yang, Y.; Joralmon, D.; Zhu, Y.; Chen, Y.; Yuan, Y.; Xu, H.; Rong, J.; Dai, R.; Nian, Q.; Chai, Y.; Chen, Y. Limpet Tooth-Inspired Painless Microneedles Fabricated by Magnetic Field-Assisted 3D Printing. *Adv. Funct. Mater.* **2021**, *31* (5), 2003725.
(160) Cornock, R.; Beirne, S.; Thompson, B.; Wallace, G. G. Coaxial Additive Manufacture of Biomaterial Composite Scaffolds for Tissue Engineering. *Biofabrication* **2014**, *6* (2), 025002.
(161) Ravichandran, D.; Xu, W.; Franklin, R.; Kanth, N.; Jambhulkar, S.; Shukla, S.; Song, K. Fabricating Fibers of a Porous-Polystyrene Shell and Particle-Loaded Core. *Molecules* **2019**, *24* (22), 4142.
(162) Franklin, R.; Xu, W.; Ravichandran, D.; Jambhulkar, S.; Zhu, Y.; Song, K. Reinforcing Carbonized Polyacrylonitrile Fibers with Nanoscale Graphitic Interface-Layers. *J. Mater. Sci. Technol.* **2021**, *95*, 78−87.
(163) Xu, W.; Ravichandran, D.; Jambhulkar, S.; Franklin, R.; Zhu, Y.; Song, K. Bioinspired, Mechanically Robust Chemiresistor for Inline Volatile Organic Compounds Sensing. *Adv. Mater. Technol.* **2020**, *5* (10), 2000440.
(164) Xu, W.; Ravichandran, D.; Jambhulkar, S.; Zhu, Y.; Song, K. Hierarchically Structured Composite Fibers for Real Nanoscale Manipulation of Carbon Nanotubes. *Adv. Funct. Mater.* **2021**, *31* (14), 2009311.

https://doi.org/10.1021/acsanm.1c01408
ACS Appl. Nano Mater. 2021, 4, 7538−7562

(165) Liu, R. Y. F.; Jin, Y.; Hiltner, A.; Baer, E. Probing Nanoscale Polymer Interactions by Forced-Assembly. *Macromol. Rapid Commun.* **2003**, *24* (16), 943−948.
(166) Ponting, M.; Hiltner, A.; Baer, E. Polymer Nanostructures by Forced Assembly: Process, Structure, and Properties. *Macromol. Symp.* **2010**, *294* (1), 19−32.
(167) Li, X.; Mckenna, G. B.; Miquelard-Garnier, G.; Guinault, A.; Sollogoub, C.; Regnier, G.; Rozanski, A. Forced Assembly by Multilayer Coextrusion to Create Oriented Graphene Reinforced Polymer Nanocomposites. *Polymer* **2014**, *55*, 248−257.
(168) Ravichandran, D.; Xu, W.; Kakarla, M.; Jambulkar, S.; Zhu, Y.; Song, K. Multiphase Direct Ink Writing (MDIW) for Multilayered Polymer/Nanoparticle Composites. *Addit. Manuf.* **2021**, submitted.
(169) Kumar, V.; Shirke, V.; Nigam, K. D. P. Performance of Kenics Static Mixer over a Wide Range of Reynolds Number. *Chem. Eng. J.* **2008**, *139* (2), 284−295.
(170) Song, H. S.; Han, S. P. A General Correlation for Pressure Drop in a Kenics Static Mixer. *Chem. Eng. Sci.* **2005**, *60* (21), 5696−5704.
(171) Meng, H.; Jiang, X.; Yu, Y.; Wang, Z.; Wu, J. Laminar Flow and Chaotic Advection Mixing Performance in a Static Mixer with Perforated Helical Segments. *Korean J. Chem. Eng.* **2017**, *34* (5), 1328−1336.
(172) Trujillo-De Santiago, G.; Alvarez, M. M.; Samandari, M.; Prakash, G.; Chandrabhatla, G.; Rellstab-Sánchez, P. I.; Byambaa, B.; Pour Shahid Saeed Abadi, P.; Mandla, S.; Avery, R. K.; Vallejo-Arroyo, A.; Nasajpour, A.; Annabi, N.; Zhang, Y. S.; Khademhosseini, A. Chaotic Printing: Using Chaos to Fabricate Densely Packed Micro- and Nanostructures at High Resolution and Speed. *Mater. Horiz.* **2018**, *5* (5), 813−822.
(173) Vancauwenberghe, V.; Verboven, P.; Lammertyn, J.; Nicolaï, B. Development of a Coaxial Extrusion Deposition for 3D Printing of Customizable Pectin-Based Food Simulant. *J. Food Eng.* **2018**, *225*, 42−52.
(174) Olvera-Trejo, D.; Velásquez-García, L. F. Additively Manufactured MEMS Multiplexed Coaxial Electrospray Sources for High-Throughput, Uniform Generation of Core-Shell Microparticles. *Lab Chip* **2016**, *16* (21), 4121−4132.
(175) Li, X.; Zhang, J. M.; Yi, X.; Huang, Z.; Lv, P.; Duan, H. Multimaterial Microfluidic 3D Printing of Textured Composites with Liquid Inclusions. *Adv. Sci.* **2019**, *6* (3), 1800730.
(176) Emonds, S.; Kamp, J.; Borowec, J.; Roth, H.; Wessling, M. Polyelectrolyte Complex Tubular Membranes via a Salt Dilution Induced Phase Inversion Process. *Adv. Eng. Mater.* **2021**, *23* (5), 2001401.
(177) Armstrong, C. D.; Todd, N.; Alsharhan, A. T.; Bigio, D. I.; Sochol, R. D. A 3D Printed Morphing Nozzle to Control Fiber Orientation during Composite Additive Manufacturing. *Adv. Mater. Technol.* **2021**, *6* (1), 2000829.
(178) Ryu, J.; Kim, Y.; Won, D.; Kim, N.; Park, J. S.; Lee, E. K.; Cho, D.; Cho, S. P.; Kim, S. J.; Ryu, G. H.; Shin, H. A. S.; Lee, Z.; Hong, B. H.; Cho, S. Fast Synthesis of High-Performance Graphene Films by Hydrogen-Free Rapid Thermal Chemical Vapor Deposition. *ACS Nano* **2014**, *8* (1), 950−956.
(179) Khadpekar, A. J.; Khan, M.; Sose, A.; Majumder, A. Low Cost and Lithography-Free Stamp Fabrication for Microcontact Printing. *Sci. Rep.* **2019**, *9*, 1024.
(180) Park, Y. G.; Min, H.; Kim, H.; Zhexembekova, A.; Lee, C. Y.; Park, J. U. Three-Dimensional, High-Resolution Printing of Carbon Nanotube/Liquid Metal Composites with Mechanical and Electrical Reinforcement. *Nano Lett.* **2019**, *19* (8), 4866−4872.
(181) Kim, S.; Oh, J.; Jeong, D.; Bae, J. Direct Wiring of Eutectic Gallium-Indium to a Metal Electrode for Soft Sensor Systems. *ACS Appl. Mater. Interfaces* **2019**, *11* (22), 20557−20565.
(182) Chang, H.; Guo, R.; Sun, Z.; Wang, H.; Hou, Y.; Wang, Q.; Rao, W.; Liu, J. Direct Writing and Repairable Paper Flexible Electronics Using Nickel-Liquid Metal Ink. *Adv. Mater. Interfaces* **2018**, *5* (20), 1800571.
(183) Owens, C. E.; Headrick, R. J.; Williams, S. M.; Fike, A. J.; Pasquali, M.; McKinley, G. H.; Hart, A. J. Substrate-Versatile Direct-Write Printing of Carbon Nanotube-Based Flexible Conductors, Circuits, and Sensors. *Adv. Funct. Mater.* **2021**, *31* (25), 2100245.
(184) Cordonier, G. J.; Sierros, K. A. Unconventional Application of Direct Ink Writing: Surface Force-Driven Patterning of Low Viscosity Inks. *ACS Appl. Mater. Interfaces* **2020**, *12* (13), 15875−15884.
(185) Boley, J. W.; White, E. L.; Chiu, G. T. C.; Kramer, R. K. Direct Writing of Gallium-Indium Alloy for Stretchable Electronics. *Adv. Funct. Mater.* **2014**, *24* (23), 3501−3507.
(186) Siebert, L.; Wolff, N.; Ababii, N.; Terasa, M. I.; Lupan, O.; Vahl, A.; Duppel, V.; Qiu, H.; Tienken, M.; Mirabelli, M.; Sontea, V.; Faupel, F.; Kienle, L.; Adelung, R. Facile Fabrication of Semiconducting Oxide Nanostructures by Direct Ink Writing of Readily Available Metal Microparticles and Their Application as Low Power Acetone Gas Sensors. *Nano Energy* **2020**, *70*, 104420.
(187) Roach, D. J.; Yuan, C.; Kuang, X.; Li, V. C. F.; Blake, P.; Romero, M. L.; Hammel, I.; Yu, K.; Qi, H. J. Long Liquid Crystal Elastomer Fibers with Large Reversible Actuation Strains for Smart Textiles and Artificial Muscles. *ACS Appl. Mater. Interfaces* **2019**, *11* (21), 19514−19521.
(188) Liang, X.; Li, H.; Dou, J.; Wang, Q.; He, W.; Wang, C.; Li, D.; Lin, J. M.; Zhang, Y. Stable and Biocompatible Carbon Nanotube Ink Mediated by Silk Protein for Printed Electronics. *Adv. Mater.* **2020**, *32* (31), 2000165.
(189) Shahariar, H.; Kim, I.; Bhakta, R.; Jur, J. S. Direct-Write Printing Process of Conductive Paste on Fiber Bulks for Wearable Textile Heaters. *Smart Mater. Struct.* **2020**, *29*, 085018.
(190) Nechyporchuk, O.; Yu, J.; Nierstrasz, V. A.; Bordes, R. Cellulose Nanofibril-Based Coatings of Woven Cotton Fabrics for Improved Inkjet Printing with a Potential in E-Textile Manufacturing. *ACS Sustainable Chem. Eng.* **2017**, *5* (6), 4793−4801.
(191) Ching, T.; Li, Y.; Karyappa, R.; Ohno, A.; Toh, Y. C.; Hashimoto, M. Fabrication of Integrated Microfluidic Devices by Direct Ink Writing (DIW) 3D Printing. *Sens. Actuators, B* **2019**, *297*, 126609.
(192) Valentine, A. D.; Busbee, T. A.; Boley, J. W.; Raney, J. R.; Chortos, A.; Kotikian, A.; Berrigan, J. D.; Durstock, M. F.; Lewis, J. A. Hybrid 3D Printing of Soft Electronics. *Adv. Mater.* **2017**, *29* (40), 1703817.
(193) Huang, Y. A.; Ding, Y.; Bian, J.; Su, Y.; Zhou, J.; Duan, Y.; Yin, Z. Hyper-Stretchable Self-Powered Sensors Based on Electrohydrodynamically Printed, Self-Similar Piezoelectric Nano/Microfibers. *Nano Energy* **2017**, *40*, 432−439.
(194) Zhang, M.; Wang, Y.; Jian, M.; Wang, C.; Liang, X.; Niu, J.; Zhang, Y. Spontaneous Alignment of Graphene Oxide in Hydrogel during 3D Printing for Multistimuli-Responsive Actuation. *Adv. Sci.* **2020**, *7* (6), 1903048.
(195) Chen, B.; Jiang, Y.; Tang, X.; Pan, Y.; Hu, S. Fully Packaged Carbon Nanotube Supercapacitors by Direct Ink Writing on Flexible Substrates. *ACS Appl. Mater. Interfaces* **2017**, *9* (34), 28433−28440.
(196) Muth, J. T.; Vogt, D. M.; Truby, R. L.; Mengüç, Y.; Kolesky, D. B.; Wood, R. J.; Lewis, J. A. Embedded 3D Printing of Strain Sensors within Highly Stretchable Elastomers. *Adv. Mater.* **2014**, *26* (36), 6307−6312.
(197) Ciui, B.; Tertiş, M.; Cernat, A.; Săndulescu, R.; Wang, J.; Cristea, C. Finger-Based Printed Sensors Integrated on a Glove for On-Site Screening of Pseudomonas Aeruginosa Virulence Factors. *Anal. Chem.* **2018**, *90* (12), 7761−7768.
(198) Bandodkar, A. J.; You, J. M.; Kim, N. H.; Gu, Y.; Kumar, R.; Mohan, A. M. V.; Kurniawan, J.; Imani, S.; Nakagawa, T.; Parish, B.; Parthasarathy, M.; Mercier, P. P.; Xu, S.; Wang, J. Soft, Stretchable, High Power Density Electronic Skin-Based Biofuel Cells for Scavenging Energy from Human Sweat. *Energy Environ. Sci.* **2017**, *10* (7), 1581−1589.
(199) Yin, L.; Lv, J.; Wang, J. Structural Innovations in Printed, Flexible, and Stretchable Electronics. *Adv. Mater. Technol.* **2020**, *5* (11), 2000694.

https://doi.org/10.1021/acsanm.1c01408
ACS Appl. Nano Mater. 2021, 4, 7538−7562

(200) Tian, K.; Bae, J.; Bakarich, S. E.; Yang, C.; Gately, R. D.; Spinks, G. M.; In het Panhuis, M.; Suo, Z.; Vlassak, J. J. 3D Printing of Transparent and Conductive Heterogeneous Hydrogel-Elastomer Systems. *Adv. Mater.* **2017**, *29* (10), 1604827.
(201) Lee, H. B.; Meeseepong, M.; Trung, T. Q.; Kim, B. Y.; Lee, N. E. A Wearable Lab-on-a-Patch Platform with Stretchable Nanostructured Biosensor for Non-Invasive Immunodetection of Biomarker in Sweat. *Biosens. Bioelectron.* **2020**, *156*, 112133.
(202) Mo, F.; Liang, G.; Huang, Z.; Li, H.; Wang, D.; Zhi, C. An Overview of Fiber-Shaped Batteries with a Focus on Multifunctionality, Scalability, and Technical Difficulties. *Adv. Mater.* **2020**, *32* (5), 1902151.
(203) Chakraborty, S.; Biswas, M. C. 3D Printing Technology of Polymer-Fiber Composites in Textile and Fashion Industry: A Potential Roadmap of Concept to Consumer. *Compos. Struct.* **2020**, *248*, 112562.
(204) Postiglione, G.; Natale, G.; Griffini, G.; Levi, M.; Turri, S. Conductive 3D Microstructures by Direct 3D Printing of Polymer/Carbon Nanotube Nanocomposites via Liquid Deposition Modeling. *Composites, Part A* **2015**, *76*, 110−114.
(205) Chen, J.; Xu, L.; Yang, M.; Chen, X.; Chen, X.; Hong, W. Highly Stretchable Photonic Crystal Hydrogels for a Sensitive Mechanochromic Sensor and Direct Ink Writing. *Chem. Mater.* **2019**, *31*, 8918−8926.
(206) Domínguez-Robles, J.; Mancinelli, C.; Mancuso, E.; García-Romero, I.; Gilmore, B. F.; Casettari, L.; Larrañeta, E.; Lamprou, D. A. 3D Printing of Drug-Loaded Thermoplastic Polyurethane Meshes: A Potential Material for Soft Tissue Reinforcement in Vaginal Surgery. *Pharmaceutics* **2020**, *12*, 63.
(207) Gao, T.; Yang, Z.; Chen, C.; Li, Y.; Fu, K.; Dai, J.; Hitz, E. M.; Xie, H.; Liu, B.; Song, J.; Yang, B.; Hu, L. Three-Dimensional Printed Thermal Regulation Textiles. *ACS Nano* **2017**, *11* (11), 11513−11520.
(208) Guiney, L. M.; Mansukhani, N. D.; Jakus, A. E.; Wallace, S. G.; Shah, R. N.; Hersam, M. C. Three-Dimensional Printing of Cytocompatible, Thermally Conductive Hexagonal Boron Nitride Nanocomposites. *Nano Lett.* **2018**, *18* (6), 3488−3493.
(209) You, X.; Yang, J.; Wang, M.; Zhou, H.; Gao, L.; Hu, J.; Zhang, X.; Dong, S. Novel Graphene Planar Architecture with Ultrahigh Stretchability and Sensitivity. *ACS Appl. Mater. Interfaces* **2020**, *12* (16), 18913−18923.
(210) Khan, R. R.; Kang, S. W. Highly Sensitive Multi-Channel IDC Sensor Array for Low Concentration Taste Detection. *Sensors* **2015**, *15* (6), 13201−13221.
(211) Wang, Z.; Zhang, Q.; Long, S.; Luo, Y.; Yu, P.; Tan, Z.; Bai, J.; Qu, B.; Yang, Y.; Shi, J.; Zhou, H.; Xiao, Z. Y.; Hong, W.; Bai, H. Three-Dimensional Printing of Polyaniline/Reduced Graphene Oxide Composite for High-Performance Planar Supercapacitor. *ACS Appl. Mater. Interfaces* **2018**, *10* (12), 10437−10444.
(212) Sun, K.; Wei, T. S.; Ahn, B. Y.; Seo, J. Y.; Dillon, S. J.; Lewis, J. A. 3D Printing of Interdigitated Li-Ion Microbattery Architectures. *Adv. Mater.* **2013**, *25* (33), 4539−4543.
(213) Rocha, V. G.; García-Tuñón, E.; Botas, C.; Markoulidis, F.; Feilden, E.; D'Elia, E.; Ni, N.; Shaffer, M.; Saiz, E. Multimaterial 3D Printing of Graphene-Based Electrodes for Electrochemical Energy Storage Using Thermoresponsive Inks. *ACS Appl. Mater. Interfaces* **2017**, *9* (42), 37136−37145.
(214) Singh, M.; Nanda, H. S.; O'Rorke, R. D.; Jakus, A. E.; Shah, A. H.; Shah, R. N.; Webster, R. D.; Steele, T. W. J. Voltaglue Bioadhesives Energized with Interdigitated 3D-Graphene Electrodes. *Adv. Healthcare Mater.* **2018**, *7* (21), 1800538.
(215) Rewatkar, P.; Goel, S. 3D Printed Bioelectrodes for Enzymatic Biofuel Cell: Simple, Rapid, Optimized and Enhanced Approach. *IEEE Trans. Nanobioscience* **2020**, *19*, 4−10.
(216) Zhou, L.-y.; Fu, J.-z.; Gao, Q.; Zhao, P.; He, Y. All-Printed Flexible and Stretchable Electronics with Pressing or Freezing Activatable Liquid-Metal-Silicone Inks. *Adv. Funct. Mater.* **2020**, *30* (3), 1906683.
(217) Zhang, Y.; Yan, Z.; Nan, K.; Xiao, D.; Liu, Y.; Luan, H.; Fu, H.; Wang, X.; Yang, Q.; Wang, J.; Ren, W.; Si, H.; Liu, F.; Yang, L.; Li, H.; Wang, J.; Guo, X.; Luo, H.; Wang, L.; Huang, Y.; Rogers, J. A. A Mechanically Driven Form of Kirigami as a Route to 3D Mesostructures in Micro/Nanomembranes. *Proc. Natl. Acad. Sci. U. S. A.* **2015**, *112* (38), 11757−11764.
(218) Goss, D.; Mistry, Y.; Niverty, S.; Noe, C.; Santhanam, B.; Ozturk, C.; Penick, C. A.; Lee, C.; Chawla, N.; Grishin, A.; Shyam, V.; Bhate, D. Bioinspired Honeycomb Core Design: An Experimental Study of the Role of Corner Radius, Coping and Interface. *Biomimetics* **2020**, *5* (4), 59.
(219) Lipton, J. I.; Maccurdy, R.; Manchester, Z.; Chin, L.; Cellucci, D.; Rus, D. Handedness in Shearing Auxetics Creates Rigid and Compliant Structures. *Science (Washington, DC, U. S.)* **2018**, *360* (6389), 632−635.
(220) Liu, Z.; Du, H.; Li, J.; Lu, L.; Li, Z. Y.; Fang, N. X. Nano-Kirigami with Giant Optical Chirality. *Sci. Adv.* **2018**, *4* (7), No. eaat4436.
(221) Gibson, L. J.; Ashby, M. F. The Mechanics Cellular Materials of Three-Dimensional Cellular Materials. *Proc. R. Soc. L.* **1982**, *A382*, 43−59.
(222) Compton, B. G.; Lewis, J. A. 3D-Printing of Lightweight Cellular Composites. *Adv. Mater.* **2014**, *26* (34), 5930−5935.
(223) Lamoureux, A.; Lee, K.; Shlian, M.; Forrest, S. R.; Shtein, M. Dynamic Kirigami Structures for Integrated Solar Tracking. *Nat. Commun.* **2015**, *6*, 8092.
(224) Lv, Z.; Luo, Y.; Tang, Y.; Wei, J.; Zhu, Z.; Zhou, X.; Li, W.; Zeng, Y.; Zhang, W.; Zhang, Y.; Qi, D.; Pan, S.; Loh, X. J.; Chen, X. Editable Supercapacitors with Customizable Stretchability Based on Mechanically Strengthened Ultralong MnO2 Nanowire Composite. *Adv. Mater.* **2018**, *30* (2), 1704531.
(225) Hu, N.; Chen, D.; Wang, D.; Huang, S.; Trase, I.; Grover, H. M.; Yu, X.; Zhang, J. X. J.; Chen, Z. Stretchable Kirigami Polyvinylidene Difluoride Thin Films for Energy Harvesting: Design, Analysis, and Performance. *Phys. Rev. Appl.* **2018**, *9* (2), 21002.
(226) Cladera, A.; Weber, B.; Leinenbach, C.; Czaderski, C.; Shahverdi, M.; Motavalli, M. Iron-Based Shape Memory Alloys for Civil Engineering Structures: An Overview. *Constr. Build. Mater.* **2014**, *63*, 281−293.
(227) Santo, L.; Quadrini, F.; Accettura, A.; Villadei, W. Shape Memory Composites for Self-Deployable Structures in Aerospace Applications. *Procedia Eng.* **2014**, *88*, 42−47.
(228) Hu, J.; Meng, H.; Li, G.; Ibekwe, S. I. A Review of Stimuli-Responsive Polymers for Smart Textile Applications. *Smart Mater. Struct.* **2012**, *21* (5), 053001.
(229) Montgomery, M.; Ahadian, S.; Davenport Huyer, L.; Lo Rito, M.; Civitarese, R. A.; Vanderlaan, R. D.; Wu, J.; Reis, L. A.; Momen, A.; Akbari, S.; Pahnke, A.; Li, R. K.; Caldarone, C. A.; Radisic, M. Flexible Shape-Memory Scaffold for Minimally Invasive Delivery of Functional Tissues. *Nat. Mater.* **2017**, *16* (10), 1038−1046.
(230) Cera, L.; Gonzalez, G. M.; Liu, Q.; Choi, S.; Chantre, C. O.; Lee, J.; Gabardi, R.; Choi, M. C.; Shin, K.; Parker, K. K. A Bioinspired and Hierarchically Structured Shape-Memory Material. *Nat. Mater.* **2021**, *20* (2), 242−249.
(231) Ahn, B. Y.; Shoji, D.; Hansen, C. J.; Hong, E.; Dunand, D. C.; Lewis, J. A. Printed Origami Structures. *Adv. Mater.* **2010**, *22* (20), 2251−2254.
(232) Liu, G.; Zhao, Y.; Wu, G.; Lu, J. Origami and 4D Printing of Elastomer-Derived Ceramic Structures. *Sci. Adv.* **2018**, *4* (8), No. eaat0641.
(233) Wei, H.; Zhang, Q.; Yao, Y.; Liu, L.; Liu, Y.; Leng, J. Direct-Write Fabrication of 4D Active Shape-Changing Structures Based on a Shape Memory Polymer and Its Nanocomposite. *ACS Appl. Mater. Interfaces* **2017**, *9* (1), 876−883.
(234) Kotikian, A.; Truby, R. L.; Boley, J. W.; White, T. J.; Lewis, J. A. 3D Printing of Liquid Crystal Elastomeric Actuators with Spatially Programed Nematic Order. *Adv. Mater.* **2018**, *30* (10), 1706164.
(235) Chen, T.; Bakhshi, H.; Liu, L.; Ji, J.; Agarwal, S. Combining 3D Printing with Electrospinning for Rapid Response and Enhanced

https://doi.org/10.1021/acsanm.1c01408
ACS Appl. Nano Mater. 2021, 4, 7538−7562

Designability of Hydrogel Actuators. *Adv. Funct. Mater.* **2018**, *28* (19), 1800514.
(236) Mao, Z.; Zhu, K.; Pan, L.; Liu, G.; Tang, T.; He, Y.; Huang, J.; Hu, J.; Chan, K. W. Y.; Lu, J. Direct-Ink Written Shape-Morphing Film with Rapid and Programmable Multimotion. *Adv. Mater. Technol.* **2020**, *5* (2), 1900974.
(237) Kim, Y.; Yuk, H.; Zhao, R.; Chester, S. A.; Zhao, X. Printing Ferromagnetic Domains for Untethered Fast-Transforming Soft Materials. *Nature* **2018**, *558* (14), 274.
(238) Sydney Gladman, A.; Matsumoto, E. A.; Nuzzo, R. G.; Mahadevan, L.; Lewis, J. A. Biomimetic 4D Printing. *Nat. Mater.* **2016**, *15* (4), 413−418.
(239) Su, R.; Wen, J.; Su, Q.; Wiederoder, M. S.; Koester, S. J.; Uzarski, J. R.; McAlpine, M. C. 3D Printed Self-Supporting Elastomeric Structures for Multifunctional Microfluidics. *Sci. Adv.* **2020**, *6* (41), No. eabc9846.
(240) Wang, J.; Yang, S.; Ding, P.; Cao, X.; Zhang, Y.; Cao, S.; Zhang, K.; Kong, S.; Zhou, Y.; Wang, X.; Li, D.; Kong, D. Omnidirectional Printing of Soft Elastomer for Liquid-State Stretchable Electronics. *ACS Appl. Mater. Interfaces* **2019**, *11* (20), 18590−18598.
(241) Luo, G.; Yu, Y.; Yuan, Y.; Chen, X.; Liu, Z.; Kong, T. Freeform, Reconfigurable Embedded Printing of All-Aqueous 3D Architectures. *Adv. Mater.* **2019**, *31* (49), 1904631.
(242) Hajash, K.; Sparrman, B.; Guberan, C.; Laucks, J.; Tibbits, S. Large-Scale Rapid Liquid Printing. *3D Print. Addit. Manuf.* **2017**, *4* (3), 123−131.
(243) Wu, W.; Deconinck, A.; Lewis, J. A. Omnidirectional Printing of 3D Microvascular Networks. *Adv. Mater.* **2011**, *23* (24), H178−H183.
(244) Liang, Z.; Pei, Y.; Chen, C.; Jiang, B.; Yao, Y.; Xie, H.; Jiao, M.; Chen, G.; Li, T.; Yang, B.; Hu, L. General, Vertical, Three-Dimensional Printing of Two-Dimensional Materials with Multiscale Alignment. *ACS Nano* **2019**, *13* (11), 12653−12661.
(245) Tomaskovic-Crook, E.; Zhang, P.; Ahtiainen, A.; Kaisvuo, H.; Lee, C. Y.; Beirne, S.; Aqrawe, Z.; Svirskis, D.; Hyttinen, J.; Wallace, G. G.; Travas-Sejdic, J.; Crook, J. M. Human Neural Tissues from Neural Stem Cells Using Conductive Biogel and Printed Polymer Microelectrode Arrays for 3D Electrical Stimulation. *Adv. Healthcare Mater.* **2019**, *8* (15), 1900425.
(246) Guo, W.; Liu, Y.; Sun, Y.; Wang, Y.; Qin, W.; Zhao, B.; Liang, Z.; Jiang, L. Vertical 3D Printed Forest-Inspired Hierarchical Plasmonic Superstructure for Photocatalysis. *Adv. Funct. Mater.* **2021**, *31* (23), 2100768.
(247) Nan, B.; Galindo-Rosales, F. J.; Ferreira, J. M. F. 3D Printing Vertically: Direct Ink Writing Free-Standing Pillar Arrays. *Mater. Today* **2020**, *35*, 16−24.
(248) Gibson, L. J. The Hierarchical Structure and Mechanics of Plant Materials. *J. R. Soc., Interface* **2012**, *9* (76), 2749−2766.
(249) Tao, Y.; Pan, L.; Liu, D.; Li, P. A Case Study: Mechanical Modeling Optimization of Cellular Structure Fabricated Using Wood Flour-Filled Polylactic Acid Composites with Fused Deposition Modeling. *Compos. Struct.* **2019**, *216*, 360−365.
(250) Varischetti, J.; Jang, J. S.; Gibson, R. F.; Suhr, J. Effect of Filler Waviness and Orientation on the Damping Behavior of CNF-Reinforced Epoxy Composites. *J. Mater. Sci.* **2013**, *48* (2), 832−840.
(251) Gibson, L. J.; Ashby, M. F.; Harley, B. A. *Cellular Materials in Nature and Medicine*; Cambridge University Press, 2010.
(252) Vogli, E.; Sieber, H.; Greil, P. Biomorphic SiC-Ceramic Prepared by Si-Vapor Phase Infiltration of Wood. *J. Eur. Ceram. Soc.* **2002**, *22* (14−15), 2663−2668.
(253) Simone, A. E.; Gibson, L. J. Effects of Solid Distribution on the Stiffness. *Acta Mater.* **1998**, *46* (6), 2139−2150.
(254) Mondal, D. P.; Goel, M. D.; Das, S. Effect of Strain Rate and Relative Density on Compressive Deformation Behaviour of Closed Cell Aluminum-Fly Ash Composite Foam. *Mater. Eng.* **2009**, *30* (4), 1268−1274.
(255) Ashby, M. F.; Gibson, L. J. Cellular Solids: Structure and Properties. *Press Synd. Univ. Cambridge, Cambridge, UK* **1997**, 175−231.
(256) Gariboldi, M. I.; Best, S. M. Effect of Ceramic Scaffold Architectural Parameters on Biological Response. *Front. Bioeng. Biotechnol.* **2015**, *3*, 151.
(257) Kolesky, D. B.; Truby, R. L.; Gladman, A. S.; Busbee, T. A.; Homan, K. A.; Lewis, J. A. 3D Bioprinting of Vascularized, Heterogeneous Cell-Laden Tissue Constructs. *Adv. Mater.* **2014**, *26* (19), 3124−3130.
(258) Sun, L.; Parker, S. T.; Syoji, D.; Wang, X.; Lewis, J. A.; Kaplan, D. L. Direct-Write Assembly of 3D Silk/Hydroxyapatite Scaffolds for Bone Co-Cultures. *Adv. Healthcare Mater.* **2012**, *1* (6), 729−735.
(259) Mccracken, J. M.; Badea, A.; Kandel, M. E.; Gladman, A. S.; Wetzel, D. J.; Popescu, G.; Lewis, J. A.; Nuzzo, R. G. Programming Mechanical and Physicochemical Properties of 3D Hydrogel Cellular Microcultures via Direct Ink Writing. *Adv. Healthcare Mater.* **2016**, *5* (9), 1025−1039.
(260) Lewis, P. L.; Green, R. M.; Shah, R. N. 3D-Printed Gelatin Scaffolds of Differing Pore Geometry Modulate Hepatocyte Function and Gene Expression. *Acta Biomater.* **2018**, *69*, 63−70.
(261) Wang, J.; Sun, Q.; Gao, X.; Wang, C.; Li, W.; Holness, F. B.; Zheng, M.; Li, R.; Price, A. D.; Sun, X.; Sham, T. K.; Sun, X. Toward High Areal Energy and Power Density Electrode for Li-Ion Batteries via Optimized 3D Printing Approach. *ACS Appl. Mater. Interfaces* **2018**, *10* (46), 39794−39801.
(262) Lin, X.; Wang, J.; Gao, X.; Wang, S.; Sun, Q.; Luo, J.; Zhao, C.; Zhao, Y.; Yang, X.; Wang, C.; Li, R.; Sun, X. 3D Printing of Free-Standing "O 2 Breathable" Air Electrodes for High-Capacity and Long-Life Na-O 2 Batteries. *Chem. Mater.* **2020**, *32* (7), 3018−3027.
(263) Lacey, S. D.; Kirsch, D. J.; Li, Y.; Morgenstern, J. T.; Zarket, B. C.; Yao, Y.; Dai, J.; Garcia, L. Q.; Liu, B.; Gao, T.; Xu, S.; Raghavan, S. R.; Connell, J. W.; Lin, Y.; Hu, L. Extrusion-Based 3D Printing of Hierarchically Porous Advanced Battery Electrodes. *Adv. Mater.* **2018**, *30* (12), 1705651.
(264) Gong, Y.; Yang, S.; Zhan, L.; Ma, L.; Vajtai, R.; Ajayan, P. M. A Bottom-up Approach to Build 3D Architectures from Nanosheets for Superior Lithium Storage. *Adv. Funct. Mater.* **2014**, *24*, 125−130.
(265) You, X.; Yang, J.; Feng, Q.; Huang, K.; Zhou, H.; Hu, J.; Dong, S. Three-Dimensional Graphene-Based Materials by Direct Ink Writing Method for Lightweight Application. *Int. J. Light. Mater. Manuf.* **2018**, *1* (2), 96−101.
(266) Shen, K.; Mei, H.; Li, B.; Ding, J.; Yang, S. 3D Printing Sulfur Copolymer-Graphene Architectures for Li-S Batteries. *Adv. Energy Mater.* **2018**, *8*, 1701527.
(267) Chen, J.; Huang, X.; Zhu, Y.; Jiang, P. Cellulose Nanofiber Supported 3D Interconnected BN Nanosheets for Epoxy Nanocomposites with Ultrahigh Thermal Management Capability. *Adv. Funct. Mater.* **2017**, *27* (5), 1604754.
(268) Li, V. C. F.; Dunn, C. K.; Zhang, Z.; Deng, Y.; Qi, H. J. Direct Ink Write (DIW) 3D Printed Cellulose Nanocrystal Aerogel Structures. *Sci. Rep.* **2017**, *7*, 8018.
(269) Zhu, C.; Han, T. Y. J.; Duoss, E. B.; Golobic, A. M.; Kuntz, J. D.; Spadaccini, C. M.; Worsley, M. A. Highly Compressible 3D Periodic Graphene Aerogel Microlattices. *Nat. Commun.* **2015**, *6*, 6962.
(270) Yang, J.; Wang, H.; Zhou, B.; Shen, J.; Zhang, Z.; Du, A. Versatile Direct Writing of Aerogel-Based Sol-Gel Inks. *Langmuir* **2021**, *37* (6), 2129−2139.
(271) Chen, B.; Tang, W.; Jiang, T.; Zhu, L.; Chen, X.; He, C.; Xu, L.; Guo, H.; Lin, P.; Li, D.; Shao, J.; Wang, Z. L. Three-Dimensional Ultraflexible Triboelectric Nanogenerator Made by 3D Printing. *Nano Energy* **2018**, *45*, 380−389.
(272) Truby, R. L.; Wehner, M.; Grosskopf, A. K.; Vogt, D. M.; Uzel, S. G. M.; Wood, R. J.; Lewis, J. A. Soft Somatosensitive Actuators via Embedded 3D Printing. *Adv. Mater.* **2018**, *30* (15), 1706383.
(273) Hong, S.; Sycks, D.; Chan, H. F.; Lin, S.; Lopez, G. P.; Guilak, F.; Leong, K. W.; Zhao, X. 3D Printing of Highly Stretchable and

https://doi.org/10.1021/acsanm.1c01408
ACS Appl. Nano Mater. 2021, 4, 7538−7562

Tough Hydrogels into Complex, Cellularized Structures. *Adv. Mater.* **2015**, *27* (27), 4035−4040.
(274) Guo, S. Z.; Qiu, K.; Meng, F.; Park, S. H.; McAlpine, M. C. 3D Printed Stretchable Tactile Sensors. *Adv. Mater.* **2017**, *29* (27), 1701218.
(275) Chen, B.; Tang, W.; Jiang, T.; Zhu, L.; Chen, X.; He, C.; Xu, L.; Guo, H.; Lin, P.; Li, D.; Shao, J.; Wang, Z. L. Three-Dimensional Ultraflexible Triboelectric Nanogenerator Made by 3D Printing. *Nano Energy* **2018**, *45*, 380−389.
(276) Galliker, P.; Schneider, J.; Eghlidi, H.; Kress, S.; Sandoghdar, V.; Poulikakos, D. Direct Printing of Nanostructures by Electrostatic Autofocussing of Ink Nanodroplets. *Nat. Commun.* **2012**, *3*, 890.
(277) Yuk, H.; Zhao, X. A New 3D Printing Strategy by Harnessing Deformation, Instability, and Fracture of Viscoelastic Inks. *Adv. Mater.* **2018**, *30* (6), 1704028.
(278) Chen, M.; Hu, S.; Zhou, Z.; Huang, N.; Lee, S.; Zhang, Y.; Cheng, R.; Yang, J.; Xu, Z.; Liu, Y.; Lee, H.; Huan, X.; Feng, S.-P.; Shum, H. C.; Chan, B. P.; Seol, S. K.; Pyo, J.; Tae Kim, J. Three-Dimensional Perovskite Nanopixels for Ultrahigh-Resolution Color Displays and Multilevel Anticounterfeiting. *Nano Lett.* **2021**, *21* (12), 5186−5194.
(279) Chen, M.; Xu, Z.; Kim, J. H.; Seol, S. K.; Kim, J. T. Meniscus-on-Demand Parallel 3D Nanoprinting. *ACS Nano* **2018**, *12* (5), 4172−4177.
(280) Tumbleston, J. R.; Shirvanyants, D.; Ermoshkin, N.; Janusziewicz, R.; Johnson, A. R.; Kelly, D.; Chen, K.; Pinschmidt, R.; Rolland, J. P.; Ermoshkin, A.; Samulski, E. T.; DeSimone, J. M. Continuous Liquid Interface Production of 3D Objects. *Science (Washington, DC, U. S.)* **2015**, *347* (6228), 1349−1352.

https://doi.org/10.1021/acsanm.1c01408
ACS Appl. Nano Mater. 2021, 4, 7538−7562